

Magnetic resonance with squeezed microwaves

A. Bienfait¹, P. Campagne-Ibarcq¹, A. Holm-Kiilerich², X. Zhou^{1,3}, S. Probst¹, J.J. Pla⁴,
T. Schenkel⁵, D. Vion¹, D. Esteve¹, J.J.L. Morton⁶, K. Moelmer², and P. Bertet¹

¹*Quantronics group, SPEC, CEA, CNRS, Université Paris-Saclay,
CEA Saclay 91191 Gif-sur-Yvette Cedex, France*

²*Department of Physics and Astronomy, Aarhus University,
Ny Munkegade 120, DK-8000 Aarhus C, Denmark*

³*Institute of Electronics Microelectronics and Nanotechnology,
CNRS UMR 8520, ISEN Department, Avenue Poincaré,
CS 60069, 59652 Villeneuve d'Ascq Cedex, France*

⁴*School of Electrical Engineering and Telecommunications,
University of New South Wales, Anzac Parade, Sydney, NSW 2052, Australia*

⁵*Accelerator Technology and Applied Physics Division,
Lawrence Berkeley National Laboratory,
Berkeley, California 94720, USA and*

⁶*London Centre for Nanotechnology, University College London,
London WC1H 0AH, United Kingdom*

(Dated: October 12, 2016)

Although vacuum fluctuations appear to represent a fundamental limit to the sensitivity of electromagnetic field measurements, it is possible to overcome them by using so-called squeezed states. In such states, the noise in one field quadrature is reduced below the vacuum level while the other quadrature becomes correspondingly more noisy, as required by Heisenberg’s uncertainty principle. Squeezed optical fields have been proposed [1] and demonstrated [2, 3] to enhance the sensitivity of interferometric measurements beyond the photon shot-noise limit, with applications in gravitational wave detection [4, 5]. They have also been used to increase the sensitivity of atomic absorption spectroscopy [6], imaging [7], atom-based magnetometry [8], and particle tracking in biological systems [9]. At microwave frequencies, cryogenic temperatures are required for the electromagnetic field to be in its vacuum state. Squeezed microwaves have been produced [10], used for fundamental studies of light-matter interaction [11–13] and for enhanced sensing of a mechanical resonator [14], and proposed to enhance the sensitivity of the readout of superconducting qubits [15, 16]. Here we report the use of squeezed microwave fields to enhance the sensitivity of magnetic resonance spectroscopy of an ensemble of electronic spins. Our scheme consists in sending a squeezed vacuum state to the input of a cavity containing the spins while they are emitting an echo, with the phase of the squeezed quadrature aligned with the phase of the echo. We demonstrate a total noise reduction of 1.2 dB at the spectrometer output due to the squeezing. These results provide a motivation to examine the application of the full arsenal of quantum metrology [17] to magnetic resonance detection.

The detection and characterisation of spins in a sample by magnetic resonance spectroscopy has numerous applications in materials science, biochemistry, and quantum information processing. Pulsed magnetic resonance proceeds by detecting weak microwave signals emitted by spins resonant with a cavity in which the sample is embedded. The noise present in these signals determines the spectrometer sensitivity and is ultimately limited by the fluctuations in the microwave field at the cavity output. The thermal contribution to these fluctuations can be removed by lowering the temperature T of the sample and cavity such that $k_B T \ll \hbar \omega_s$ (ω_s being the spin resonance frequency, k_B the Boltzmann constant and \hbar the reduced Planck’s constant) [18]. In this low-temperature limit, only the quantum

fluctuations of the electromagnetic field remain, as required by Heisenberg's uncertainty principle: denoting \hat{X} and \hat{Y} to be the two quadratures of the field in dimensionless units (i.e. such that $\langle \hat{X}^2 \rangle + \langle \hat{Y}^2 \rangle = N + 1/2$, N being the average photon number), then the variances in each must satisfy the inequality $\delta X^2 \delta Y^2 \geq 1/16$. In the vacuum state, fluctuations in both quadratures have the same magnitude: $\delta X^2 = \delta Y^2 = 1/4$. It is possible, however, to engineer so-called squeezed states in which the variance in one quadrature (called the squeezed quadrature) is reduced below the vacuum level ($1/4$), at the expense of an increase in variance in the other quadrature.

To understand how squeezed states can be used to improve the sensitivity of an electron-spin resonance (ESR) spectrometer beyond that determined by vacuum fluctuations (the so-called standard quantum limit), consider the schematic description in Fig. 1. A single-port lossless resonator of frequency ω_0 containing the sample is coupled with a rate κ_C to the measurement line that supports incoming (\hat{b}_{in}) and outgoing (\hat{b}_{out}) field modes. A dc magnetic field B_0 is applied to tune the spin frequency into resonance with the cavity. A Hahn echo sequence [19] consisting of a $\pi/2$ pulse at time $t = 0$ followed by a π pulse at $t = \tau$ leads to rephasing of the spins at $t = 2\tau$ and, whenever $\omega_s \approx \omega_0$, to the emission of an echo on one field quadrature (that we take here to be \hat{X}) in the output measurement line. This echo is then amplified noiselessly with a quantum-limited amplifier (see below), and detected by coherently mixing it with a local oscillator whose phase is adjusted such that the echo signal is on the $I(t)$ output quadrature. The noise accompanying the echo arises from the (amplified) fluctuations in b_{in} , the input field reflected by the cavity into the output mode; it reaches the quantum limit if b_{in} is in the vacuum state. If b_{in} is instead prepared in a squeezed vacuum state with its squeezed quadrature coinciding with the \hat{X} quadrature on which the echo is emitted, the noise in $I(t)$ can be below the quantum limit (see Fig. 1), whereas the noise on the other quadrature (which bears no spin signal) is above. This qualitative argument is validated, in the case of a weakly coupled spin ensemble, by a full quantum analysis based on input-output theory (see Supplementary Information).

In our experiment, both the squeezed vacuum generation and the noiseless amplification are achieved by the same type of device: a flux-pumped JPA operated in degenerate mode [20] denoted SQZ for the squeezer and AMP for the amplifier. The JPA is a single-port resonator of frequency close to ω_0 containing a SQUID array whose flux is modulated by a pump tone at frequency $2\omega_0$ with a phase ϕ leading to a resonator frequency modu-

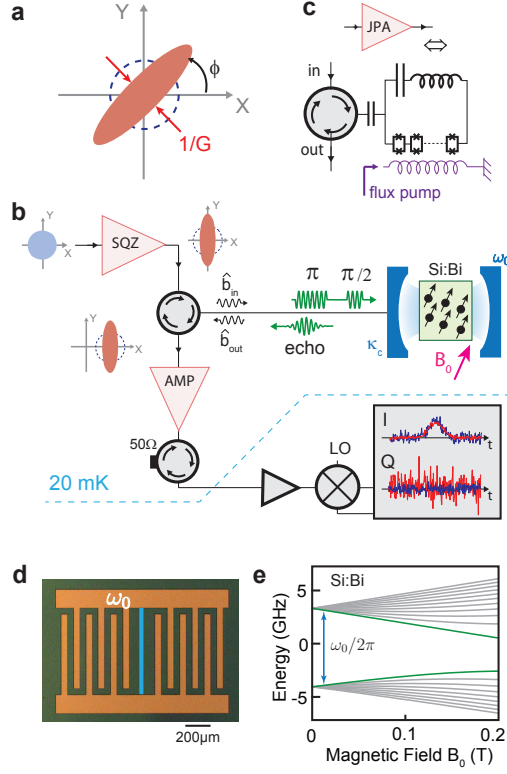


FIG. 1. Principle of squeezing-enhanced pulsed magnetic resonance and experimental setup. (a) Squeezed states exhibit fluctuations (red ellipse in the phase space) which are reduced compared to the vacuum level (blue dashed circle) on the so-called squeezed quadrature (tilted at some angle ϕ with respect to the X quadrature). (b) A JPA, denoted SQZ, produces a squeezed vacuum state which is incident on a cavity with frequency $\omega_0/2\pi = 7.3$ GHz. The cavity contains the spins to be detected, which are tuned into resonance at ω_0 by a dc magnetic field B_0 . A Hahn echo microwave pulse sequence ($\pi/2 - \tau - \pi - \tau$) is applied to the spins, leading to the emission of an echo in the detection waveguide on the X quadrature. This echo is noiselessly amplified by a second JPA denoted AMP, followed by amplification at higher temperatures and homodyne demodulation with a local oscillator phase such that $I(t)$ is proportional to $\hat{X}(t)$. The traces in the bottom right grey box, which are not real data, depict schematically the expected difference between SQZ off (blue) and SQZ on (red) output quadrature signals when the squeezed quadrature is aligned along the echo emission quadrature X ; they show that the signal-to-noise ratio is improved beyond the standard quantum limit. (c) The JPAs are superconducting LC resonators containing a SQUID array, making them tunable in flux. Pumping this flux at twice the LC frequency ($2\omega_0$) yields a parametric gain. (d) Optical micrograph of the ESR cavity, a superconducting LC resonator patterned on top of a silicon chip containing bismuth (Bi) donors. The spins of Bi donors in the immediate vicinity of the resonator inductance⁴ (colorized in blue) are detected. (e) Energy level diagram of Bi donor spins in silicon, showing the lowest frequency transition (green) used here.

lation $\propto \cos[2(\omega_0 t + \phi)]$ [20]. Parametric amplification with amplitude gain G occurs for input signals $V \cos \omega_0 t$ if $\phi = -\pi/4$, and de-amplification with gain $1/G$ if $\phi = +\pi/4$. The SQZ is a JPA acting on the vacuum at its input, generating a squeezed vacuum state with a variance reaching $1/(4G^2)$ on its squeezed quadrature, with an average photon number $N = (G^2 + G^{-2} - 2)/4$ (see [13] and Supplementary Information). The ESR cavity is a high-quality-factor superconducting LC resonator patterned on top of a silicon sample enclosed in a copper holder. The spins are bismuth donors implanted in the silicon sample, isotopically enriched in (nuclear-spin-free) ^{28}Si [21, 22] (see Fig. 1 and Supplementary Information). At low magnetic fields, due to the strong hyperfine interaction between the $S = 1/2$ electron and the $I = 9/2$ nuclear spins, multiple ESR-like transitions are allowed around 7.37 GHz; we work here on the lowest frequency transition.

We first characterise the squeezed microwave signal, keeping the spins detuned from the ESR resonator. We show in Fig. 2a the effect of pump phase (ϕ_S and ϕ_A) on the power gain (G_S and G_A) for SQZ and AMP, respectively. The gains vary sinusoidally as expected, with $G_S^2 = 6$ dB and $G_A^2 = 20$ dB for the chosen pump amplitude settings. In the remainder of this work, the local oscillator phase is set such that the quadrature maximally amplified by AMP is $I(t)$. Time traces of $I(t)$ are obtained by digitizing the signal with a bandwidth of 300 kHz, much smaller than the 3 MHz squeezing bandwidth. The variance δI^2 is shown in Fig. 2b as a function of the relative phase between the SQZ and AMP pump signals $\phi_\Delta = \phi_S - \phi_A$, with no signal at the input. As demonstrated in [23], δI^2 depends on ϕ_Δ , allowing us to experimentally determine the optimal squeezing condition $\phi_\Delta = \pi/2$. Statistical distributions of $I(t)$ are shown in the form of histograms in Fig. 2c for this optimal condition. We find the variance in the total output noise (δI_{on}^2) is reduced below that observed with the SQZ pump off (δI_{off}^2), $\delta I_{on}^2 = 0.75 \delta I_{off}^2$ (see Figs. 2b and c). Combined with calibration measurements showing that the mean number of thermal photons with SQZ off is ≤ 0.1 (see Supplementary Information), these results prove that the squeezed quadrature has its variance reduced by at least a factor 1.1 (1 dB) below the vacuum fluctuations level.

One well-known difficulty encountered when working with squeezed states is their sensitivity to losses. When the squeezed state is attenuated by η_{loss} (with $0 < \eta_{\text{loss}} < 1$ the ratio of output to input powers), the squeezed quadrature variance becomes $\eta_{\text{loss}}/(4G^2) + (1 - \eta_{\text{loss}})/4$, which implies a reduced degree of squeezing. For our experiment, the relevant microwave

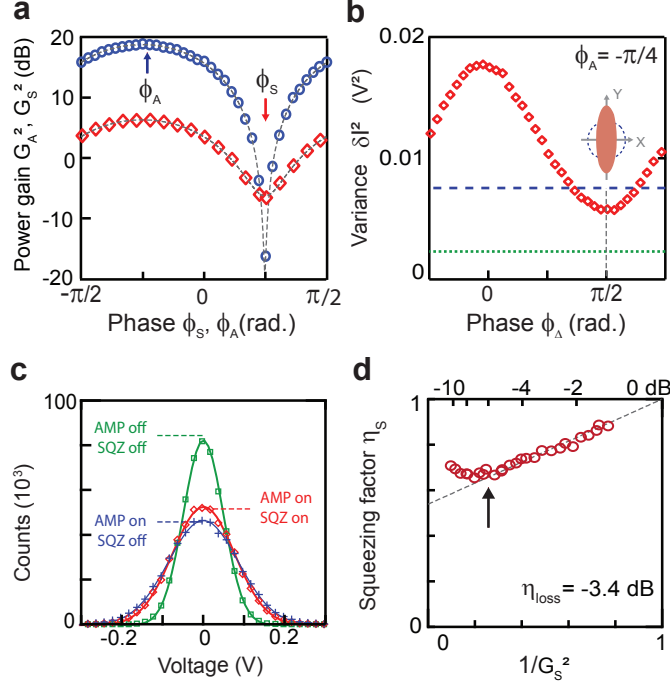


FIG. 2. Characterisation of the prepared squeezed vacuum state. (a) Gain of SQZ and AMP as a function of their pump phase ($\phi_{S,A}$, respectively) for the chosen pump amplitude settings, leading to a maximum power gain $G_S^2 = 6$ dB and $G_A^2 = 20$ dB. Optimal values for the SQZ and AMP pump phases are indicated with arrows. (b) The variance δI^2 in the noise is plotted as a function of the SQZ pump phase ϕ_S (ϕ_A being set at its optimal value) with AMP and SQZ both on (red open squares), and compared to the values obtained with AMP on and SQZ off (blue dashed line), and with AMP and SQZ both off (green dashed line). Squeezing is obtained for the optimal setting $\phi_\Delta = \pi/2$. (c) Noise histograms obtained using the optimal phases obtained above, for the cases of : AMP and SQZ both off (green open squares), AMP on and SQZ off (blue crosses), and AMP and SQZ both on (red open symbols). Gaussian fits for each are also shown (curves). (d) Using the optimal phase settings, the squeezing factor (see main text) η_S is measured as a function of the SQZ power gain (open red circles). A linear fit (dashed line) for the low-gain part of the curve indicates the microwave losses between SQZ and AMP to be $\eta_{\text{loss}} = -3.4$ dB. The black arrow indicates the gain selected in the experiment.

losses are those between SQZ and AMP, which include the insertion loss of circulators and cables, and internal losses of the SQZ and AMP devices as well as of the ESR resonator. Care was taken to minimize these losses; in particular, the coupling rate of the resonator

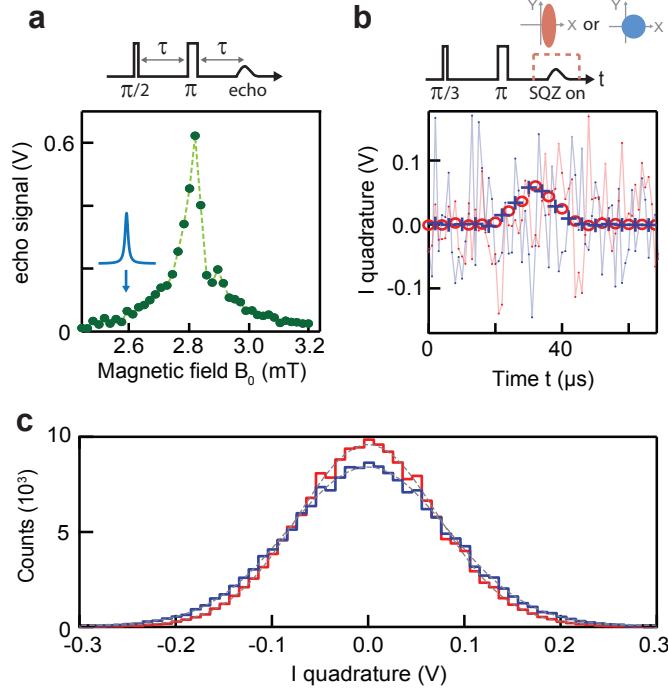


FIG. 3. Squeezing-enhanced spin-echo detection. (a) Hahn-echo detected magnetic field sweep, showing the bismuth donor resonance line broadened by strain. Blue arrow indicates the field chosen in the rest of the experiment, blue Lorentzian curve the ESR resonator linewidth. (b) Echo signals observed with SQZ off (blue) and on (red) for a single shot (lines) and averaged over 2500 traces (symbols) confirm the signal intensity is identical. The excitation pulse angle is chosen to be $\approx \pi/3$ in order to avoid saturation effects (see main text). (c) Histograms of the noise around the average signals of panel b measured with 2500 single-shot traces acquired on a $70 \mu\text{s}$ -time-window centered on the echo, with SQZ off (blue) and on (red) (see Supp. Mat.), and accompanying Gaussian fits (dashed curves). Standard deviations are 0.12V for SQZ off and 0.11V for SQZ on, confirming a reduction in the variance of the noise in the spin echo when SQZ is on.

to the output waveguide, $\kappa_C = 1.2 \cdot 10^6 \text{ s}^{-1}$, was purposely set to be much larger than the internal loss rate of resonator, $\kappa_L = 6 \cdot 10^4 \text{ s}^{-1}$ so that the losses in reflection are below 1 dB.

To determine the impact of losses on the degree of squeezing in our experiment, we measure the squeezing factor $\eta_S \equiv (\delta I_{on}^2 - \delta I_{bg}^2)/(\delta I_{off}^2 - \delta I_{bg}^2)$ as a function of G_S^2 (see Fig. 2d), δI_{bg}^2 being the variance in the background noise obtained when both SQZ and AMP are switched off. With this definition, η_S measures only the quantum noise reduction due to squeezing. For low gains ($\lesssim 5 \text{ dB}$), η_S shows the expected linear dependence with

G_S^{-2} , and the fit yields a total microwave loss $\eta_{\text{loss}} = -3.4$ dB between SQZ and AMP. At higher gains, a departure from linearity is observed, with an increase of the variance that we attribute to a Kerr non-linearity induced in the SQZ resonator by the Josephson junctions used to modulate the resonator frequency (see Supplementary Information).

Under the tests described above, the input state into AMP is a vacuum or squeezed state, in either case well below the saturation limit of the JPA. In the experiments which follow, when the spins are brought onto resonance with the cavity, this input signal additionally contains a contribution from the emission of spins during an echo. We find that AMP saturates in phase at an input power of -136 dBm (see Supplementary Information). We ensure the echo signal remains below this power by exciting the spins at the edge of the inhomogeneously broadened resonance line (effectively selecting a small number of spins) and using an excitation pulse less than $\pi/2$ in the Hahn echo sequence.

Fig. 3a shows the electron spin resonance spectrum of the Bi donor spins, obtained by measuring the spin-echo intensity as a function of magnetic field (with SQZ off). This shows the expected resonance around $B_0 = 2.8$ mT (see Fig. 1e), with the 0.1 mT linewidth primarily due to strain exerted by the aluminium wire on the underlying silicon substrate [24]. Rabi oscillations (obtained by sweeping the power of the refocusing pulse in the Hahn echo sequence) were then used to calibrate the pulses for subsequent experiments [25]. To avoid phase saturation of AMP, we set the field B_0 to 2.6 mT and used an echo sequence of the form $\frac{\pi}{3} - \tau - \pi - \tau - \text{echo}$, with $\tau = 200$ μs . The observed echo was then compared for the cases of i) SQZ off; and ii) SQZ pump switched on for a time window of 200 μs centred around the expected echo emission time. The phases of the excitation and refocusing pulses were set in such a way that the echo signal was entirely on the I quadrature aligned with the squeezed vacuum.

Time traces of the digitized $I(t)$ quadrature are shown in Fig. 3b, with the echo barely visible in single-shot traces. After averaging, the spin-echo amplitude appears to be identical for SQZ on and off, as expected. However, histograms of the noise during the echo emission (Fig. 3c) show that the data obtained with SQZ on exhibit less noise than with SQZ off — indeed, the similarity between these distributions and those obtained with no spin-echo signal (Fig. 2c) confirm that quantum fluctuations are the primary noise source in the spin echo measurements, and in both cases the variance is reduced by a factor of 0.75 when SQZ is on. As the noise reduction is obtained while maintaining constant spin-echo signal amplitude,

this demonstrates that the sensitivity of magnetic resonance detection is enhanced below the shot-noise limit using quantum squeezing.

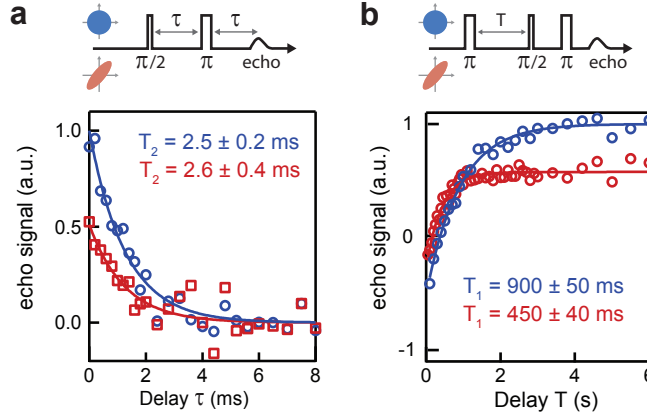


FIG. 4. Influence of squeezing on spin coherence times. (a) Coherence time T_2 measured with a Hahn echo sequence for SQZ off (blue circles) and on (red squares). The integrated echo signal is plotted as a function of the delay τ between $\pi/2$ and π pulse. Exponential fits (solid lines) yield $T_{2,off} = 2.5 \pm 0.2$ ms and $T_{2,on} = 2.6 \pm 0.4$ ms. (b) Energy relaxation time T_1 with SQZ on (blue circles) and off (red squares). Exponential fits (solid lines) yield $T_{1,off} = 900 \pm 50$ ms whereas $T_{1,on} = 450 \pm 40$ ms. Both T_1 and T_2 curves (panels a and b) have their amplitude reduced by ≈ 0.5 with SQZ on, indicating reduced spin polarisation in steady-state.

The achieved gain in sensitivity is limited by the finite degree of squeezing, due to the above-mentioned issues of JPA non-linearity and losses. Were the degree of squeezing considerably improved, the sensitivity would however not increase indefinitely because of effects both on the noise and on the signal which we have thus far neglected and briefly discuss below.

First, in addition to the quantum fluctuations of b_{in} , the output field b_{out} contains noise due to absorption and emission of the spins [26]. Negligible in our experiment, this contribution would become dominant in the limit of strong squeezing. Numerical simulations indicate that for our experimental parameters, this limits achievable sensitivity gain to a factor $\simeq 10$ (see Supplementary Information).

Second, squeezing can also affect the echo signal, due to the backaction it exerts on the spin dynamics. Indeed, in steady-state, squeezed radiation incident on a two-level system modifies its relaxation and coherence times as well as its average polarisation, as predicted

in Ref [11] and observed in recent experiments with superconducting qubits [13, 27]. To investigate these effects, we measure spin coherence and relaxation times with SQZ turned off or on during the entire experimental sequence. T_2 is found to be unaffected by squeezing (see Fig. 4a), because it is limited by non-radiative processes such as dipolar interactions [28]. The energy relaxation time T_1 however, being of radiative origin [25], is found to decrease from 0.9 s to 0.45 s (see Fig. 4b), with an overall echo amplitude diminished by the same factor 2, revealing the expected reduced spin polarisation. The reduction factor on both T_1 and polarisation is predicted by Gardiner to be $1 + 2N$ [11], yielding $N \approx 0.5$ in our experiment, compatible with the squeezed state characterisation by homodyne detection (see Fig. 2). Squeezing-induced spin depolarisation was avoided in the data shown in Fig. 3c because SQZ was only on for a short time window $\Delta t = 200 \mu\text{s}$ around the echo, much smaller than the depolarisation time which is of order $\approx T_1/(1 + 2N)$. Sensitivity could thus no longer be improved if this depolarisation time is comparable to the echo duration, i.e. if a squeezed state with an average photon number $N > T_1/(2T_E)$ was used. For our experimental parameters, this is on the order of 10^4 , corresponding to a 40 dB squeezed quadrature, which sets another upper bound of $\simeq 100$ on the sensitivity gain achievable by the use of squeezing.

We have presented a proof-of-principle demonstration of squeezing-enhanced magnetic resonance detection. While the fundamental limitations to this scheme deserve further study, our estimates show that for present-day experimental parameters, the method may bring up to an order of magnitude improvement in sensitivity provided highly squeezed microwave states can be produced and preserved during their propagation, which should become possible with the on-going development of lossless circulators [29]. Besides improving the degree of squeezing, future work could investigate the use of other non-classical states such as Schrödinger-cat states in magnetic resonance, which might bring even larger sensitivity gains [17, 30].

ACKNOWLEDGMENTS

We acknowledge technical support from P. Sénat, D. Duet, J.-C. Tack, P. Pari, P. Forget, as well as useful discussions within the Qnantronics group. We acknowledge support of the European Research Council under the European Community's Seventh Framework Pro-

gramme (FP7/2007-2013) through grant agreements No. 615767 (CIRQUSS), 279781 (ASCENT), and 630070 (quRAM), and of the C’Nano IdF project QUANTROCRYO. J.J.L.M. is supported by the Royal Society. T.S. was supported by the U. S. Department of Energy under contract DE-AC02-05CH11231. A.H.K. and K.M. acknowledge support from the Villum Foundation.

Supplementary Material: Magnetic Resonance with Squeezed Microwaves

I. THEORY: SQUEEZING AND AMPLIFICATION BY A JOSEPHSON PARAMETRIC AMPLIFIER

In the experiment, we use Josephson parametric amplifiers (JPA) to both produce a squeezed vacuum input field incident on the resonator and to amplify a single quadrature of the emitted radiation in a noiseless manner. The JPA is flux pumped at a frequency $2\omega_0$, and it is employed in a degenerate mode to act on input fields within a few MHz frequency bandwidth, $\omega \simeq \omega_0$. For a general review on parametric amplification, see [31], and let us merely establish the formalism here, focusing on the limit of broad band squeezing.

When the input is vacuum or a thermal state, the output quadrature fluctuations are squeezed along a phase direction governed by the pump phase, while a non-vanishing mean amplitude is modified by a phase sensitive amplification factor. This is captured by the transformation of the field quadrature operators with the amplitude gain coefficient G ,

$$\begin{aligned} X_{\text{out}} &= GX_{\text{in}} \\ Y_{\text{out}} &= G^{-1}Y_{\text{in}} \end{aligned} \tag{S1}$$

equivalent to the transformation of the field annihilation and creation operators ($X = \frac{1}{2}(a + a^\dagger)$, $Y = \frac{1}{2i}(a - a^\dagger)$),

$$\begin{aligned} a_{\text{out}} &= \frac{G + G^{-1}}{2}a_{\text{in}} + \frac{G - G^{-1}}{2}a_{\text{in}}^\dagger \\ a_{\text{out}}^\dagger &= (a_{\text{out}})^\dagger. \end{aligned} \tag{S2}$$

Assuming the broadband limit, and application of Eq. S1 to a vacuum or a thermal state, Eqs. S2 lead to the temporal correlations of the squeezed output field,

$$\begin{aligned} \langle a_{\text{out}}^\dagger(t)a_{\text{out}}(t') \rangle &= \left(\frac{G + G^{-1}}{2} \right)^2 \langle a_{\text{in}}^\dagger(t)a_{\text{in}}(t') \rangle + \left(\frac{G - G^{-1}}{2} \right)^2 \langle a_{\text{in}}(t)a_{\text{in}}^\dagger(t') \rangle \equiv N\delta(t - t') \\ \langle a_{\text{out}}(t)a_{\text{out}}(t') \rangle &= \frac{G + G^{-1}}{2} \frac{G - G^{-1}}{2} \left(\langle a_{\text{in}}^\dagger(t)a_{\text{in}}(t') \rangle + \langle a_{\text{in}}(t)a_{\text{in}}^\dagger(t') \rangle \right) \equiv M\delta(t - t'). \end{aligned} \tag{S3}$$

The process which thus squeezes the field quadratures by the coefficients G and G^{-1} , respectively, is characterized by a mean output photon number

$$N = \frac{G^2 + G^{-2}}{2}\bar{n} + \frac{G^2 + G^{-2} - 2}{4}, \tag{S4}$$

where \bar{n} is the input mean photon number ($\mathcal{G} \equiv \frac{G^2 + G^{-2}}{2}$ is called the power gain). The two-photon coherence

$$M = \frac{G^2 - G^{-2}}{4} (2\bar{n} + 1) \quad (\text{S5})$$

characterizes the degree of squeezing by the phase sensitive amplification. In the case of a vacuum input state, the mean output photon number is $N = \frac{G^2 + G^{-2} - 2}{4}$ and we have, $M = \sqrt{N(N + 1)}$.

If the driving modulation at $2\omega_0$ has a phase 2ϕ , the squeezing occurs for a rotated quadrature component, and is represented by a complex value, $M \rightarrow Me^{2i\phi}$ in Eqs. S3. Using the expressions in Eq. S3, we readily find that a rotated quadrature component $X_\theta = \frac{1}{2}(e^{-i\theta}a_{out} + e^{i\theta}a_{out}^\dagger)$ of the squeezed state has the variance,

$$\delta X_\theta^2 = \langle X_\theta^2 \rangle = \frac{1}{2}(N + M \cos(2(\theta - \phi))) + \frac{1}{2}. \quad (\text{S6})$$

The angles $\theta = \phi$ and $\theta = \pi/2 + \phi$ specify the principal axes of the squeezing ellipse shown in Fig.1a, along which the fluctuations are anti-squeezed and squeezed by the phase sensitive gain factors G and G^{-1} , respectively.

Applying Eq. S1 to amplify a field with mean complex amplitude $\alpha = \alpha_R + i\alpha_I$ results in an output mean signal $G\alpha_R + iG^{-1}\alpha_I$ and to the equivalent amplification of the fluctuations of the two field quadratures. *I.e.*, the amplification Eq. S1, that we apply to the output from the resonator, is unitary and maintains the signal-to-noise ratio [1].

In the case of steady state squeezing with a finite bandwidth, Δ_{sq} , the delta-function correlations in Eqs. S3 are replaced by exponential functions in the time argument $|t - t'|$ [31]. In the next section, the squeezed output fields a_{out}, a_{out}^\dagger are taken as the input to the resonator system containing the probed spin ensemble.

II. THEORY: RESONATOR OUTPUT SIGNAL AND ITS FLUCTUATIONS

We are dealing with an inhomogeneously broadened spin ensemble which is excited and refocussed by strong classical pulses and interacts with a quantized resonator mode, which is, in turn, damped through output losses and subject to a squeezed incident radiation field. By applying a simple Ansatz for the spin dynamics, we can solve this problem in the Heisenberg picture by use of the input-output formalism of quantum optics [32].

A. Input-output relation

The Heisenberg equation of motion for the annihilaton operator of a cavity field $a(t)$ is given by ($\hbar = 1$),

$$\dot{a}(t) = -i[a, H_S] - \frac{\kappa}{2}a(t) + \sqrt{\kappa}b_{\text{in}}(t), \quad (\text{S7})$$

where H_S is the Hamiltonian of the field, including its coupling to the spin system inside the cavity, and κ is the cavity damping rate (we assume in the following that the cavity loss is solely due to the resonator out-coupling port). The last term in Eq. S7 is due to the quantized radiation field incident on the cavity, and acts as a Langevin noise term which ensures that, *e.g.*, the commutator relation $[a, a^\dagger] = 1$ holds for all times.

The decay rate κ stems also from the coupling between the cavity mode and the field modes outside the cavity. It is calculated by determining first the beam-splitter like interaction between the cavity field and the input field and, subsequently, to second order in perturbation theory, the damping and Lamb shift acting back on the cavity mode. The field $b_{\text{in}}(t)$ in Eq. S7 is the freely evolved input field, unaffected by the cavity mode, while an analysis of the beam-splitter like coupling of the cavity field and the outgoing field leads to the alternative Heisenberg equation of motion,

$$\dot{a}(t) = -i[a, H_S] + \frac{\kappa}{2}a(t) - \sqrt{2\kappa}b_{\text{out}}(t), \quad (\text{S8})$$

where $b_{\text{out}}(t)$ is the output field leaving the resonator.

Together Eqs. S7, S8 yield the important input-output relation,

$$b_{\text{in}}(t) + b_{\text{out}}(t) = \sqrt{\kappa}a(t). \quad (\text{S9})$$

B. Coupling of the refocussed spin ensemble to the resonator field

Due to inhomogeneous broadening, spins prepared in coherent superposition states at a time $t = -\tau$ precess at different frequencies Δ_j - in a frame rotating with the center spin and resonator frequency - and the mean spin vector thus approaches a constant in a time $1/\Gamma$, where Γ is the width of the frequency distribution. Subject to a π pulse rotation at time $t = 0$, the distribution of spin components in the plane perpendicular to the precession axis is flipped, and if each spin continues to precess at its own frequency, the spins will all come back in phase and emit a radiation echo at the time $t = \tau$. Here we wish to examine to

what extent this echo is affected by the coupling of the spins to the resonator mode before, during and after the echo, and if the illumination of the resonator by a squeezed input field will affect the spin dynamics. As we will only record the signal in a time window around the expected echo, we shall not describe the dynamics during the initial excitation and the inversion of the spin ensemble by strong classical pulses. Instead, we assume, as the initial state of our analysis, the state just after the echo pulse at $t = 0$, where the individual spins populate superposition states with phases $\phi_j = \Delta_j \tau$, which will ideally be compensated by their subsequent phase evolution, $\exp(-i\Delta_j t)$, bringing them all in phase at time $t = \tau$.

During this time evolution, the spins couple to the cavity field, $H_S = \sum_j g(a\sigma_j^\dagger + a^\dagger\sigma_j)$, with strength g , and we shall approximate the spin lowering operators σ_j as oscillator annihilation operators, obeying the oscillator commutator relations $[\sigma_j, \sigma_k^\dagger] = \delta_{jk}$. This Holstein-Primakov approximation [33] is not good for a single spin but it is adequate to describe a system of many spins.

Equation S7 now reads,

$$\dot{a} = -ig \sum_j \sigma_j - \frac{\kappa}{2}a + \sqrt{\kappa}b_{\text{in}}(t) \quad (\text{S10})$$

and to describe the initial coherent excitation of the spins (oscillators) with complex amplitudes $\alpha \exp(i\Delta_j \tau)$, we introduce a delta-function excitation pulse in the spin equations of motion,

$$\dot{\sigma}_j = -(\gamma + i\Delta_j)\sigma_j - iga + \alpha e^{i\Delta_j \tau} \delta(t) + \sqrt{2\gamma}F_j(t) \quad (\text{S11})$$

where γ is a phenomenological spin relaxation rate, accompanied by quantum Langevin noises $F_j(t)$ acting on a reservoir field with non-vanishing commutators $[F_i(t), F_j^\dagger(t')] = \delta(t - t')\delta_{ij}$. This relaxation is introduced to represent slow coherence and excitation decay of the oscillators, and its actual value will not be significant for the parameters of the experiment described in the main text. In section IV of this Supp. Mat., we shall estimate the consequences when spin relaxation occurs on time scales comparable with the spin echo experiment.

Applying the Fourier transforms, $\tilde{f}(\omega) = \frac{1}{\sqrt{2\pi}} \int f(t)e^{-i\omega t} dt$ and $f(t) = \frac{1}{\sqrt{2\pi}} \int \tilde{f}(\omega)e^{i\omega t} d\omega$, we can write the equations of motion in algebraic form,

$$\begin{aligned} -i\omega \tilde{a}(\omega) &= -\frac{\kappa}{2}\tilde{a}(\omega) - ig \sum_j \tilde{\sigma}_j(\omega) + \sqrt{\kappa}\tilde{b}_{\text{in}}(\omega) \\ -i\omega \tilde{\sigma}_j(\omega) &= -(\gamma + i\Delta_j)\tilde{\sigma}_j(\omega) - ig\tilde{a}(\omega) + \alpha e^{i\Delta_j \tau}/\sqrt{2\pi} + \sqrt{2\gamma}\tilde{F}_j(\omega). \end{aligned} \quad (\text{S12})$$

The operator equations for the spins can be formally solved,

$$\tilde{\sigma}_j(\omega) = \frac{\alpha e^{i\Delta_j\tau}/\sqrt{2\pi} - ig\tilde{a}(\omega) + \sqrt{2\gamma}\tilde{F}_j(\omega)}{\gamma + i\Delta_j - i\omega}. \quad (\text{S13})$$

We proceed by inserting this result in the equation for the cavity field and solving

$$\tilde{a}(\omega) = \frac{-ig \sum_j \frac{\alpha}{\sqrt{2\pi}} e^{i\Delta_j\tau}/(\gamma + i\Delta_j - i\omega) + \tilde{F}_{\text{spin}}(\omega) + \sqrt{\kappa}\tilde{b}_{\text{in}}(\omega)}{\kappa/2 - i\omega + \sum_j g^2/(\gamma + i\Delta_j - i\omega)}, \quad (\text{S14})$$

where we defined $\tilde{F}_{\text{spin}}(\omega) = -ig\sqrt{2\gamma} \sum_j \tilde{F}_j(\omega)/(\gamma + i\Delta_j - i\omega)$, accounting for the contribution of the spins to the noise in the cavity field. Notice that we have $[\tilde{F}_{\text{spin}}(\omega), \tilde{F}_{\text{spin}}^\dagger(\omega')] = 2g^2\gamma \sum_j \frac{\delta(\omega-\omega')}{\gamma + i\Delta_j - i\omega}$. The expression for the resonator field is a sum of three terms: a contribution from the spin echo, and two contributions from the Langevin spin noise term and from the vacuum or squeezed input on the resonator.

C. Mean value and fluctuations of the output field

The mean value of the field operator Eq. S14 comes from the spin echo and the resulting output mean amplitude does not depend on the squeezing parameters. The noise in the output field, however, will benefit from the squeezing which causes reduced fluctuations in the amplitude measurements.

To get a feeling for the expressions, we shall now replace the sum over N_{spins} spins by an integral $\sum_j \cdot \rightarrow N_{\text{spins}} \int d\Delta f(\Delta) \cdot$, and as an example consider a Lorentzian distribution $f(\Delta) = (\Gamma/2\pi)/(\Delta^2 + \Gamma^2/4)$. The sum in the denominator of $\tilde{a}(\omega)$ can be calculated by Cauchy's integral formula, and yields $N_{\text{spins}}g^2[\Gamma/2 + \gamma + i\omega]/[(\gamma + \Gamma/2)^2 + \omega^2]$, which we rewrite as $\kappa C(\omega)/2$ introducing the frequency-dependent ensemble cooperativity $C(\omega)$. Due to the exponential factors depending on Δ , the integral replacing the sum in the numerator must be completed in the upper half of the complex plane, and yields the residues for the two poles at $\Delta = i\Gamma/2 + \omega$ and $\Delta = i\gamma + \omega$. The former contribution is negligible due to the resulting exponential factor $e^{-\Gamma\tau/2}$ evaluated at the pole (recall that τ is the echo time which occurs much later than $1/\Gamma$). The other pole, however, yields a finite value for the c-number part of the sum: $(\alpha/\sqrt{2\pi})(n\Gamma/[(i\gamma + \omega)^2 + \Gamma^2/4])e^{-\gamma\tau + i\omega\tau}$. This result makes excellent sense, the spin echo causes emission of a signal with a frequency width $\sim \Gamma/2$ and as the spins have experienced a slow decoherence until time τ , the signal is damped by the factor $e^{-\gamma\tau}$.

Finally, replacing the sum in the commutator relation of the spin noise contribution $\tilde{F}_{\text{spin}}(\omega)$ in the numerator by an integral yields $[\tilde{F}_{\text{spin}}(\omega), \tilde{F}_{\text{spin}}^\dagger(\omega')] = \kappa \text{Re}[C(\omega)] \delta(\omega - \omega')$.

Inserting the evaluated expressions, gives

$$\tilde{a}(\omega) = \frac{-2ign\alpha\Gamma e^{-\gamma\tau+i\omega\tau}}{\sqrt{2\pi}\{(i\gamma+\omega)^2+\Gamma^2/4\}\{\kappa[1+C(\omega)]-2i\omega\}} + \frac{2\tilde{F}_{\text{spin}}(\omega) + 2\sqrt{\kappa}\tilde{b}_{\text{in}}(\omega)}{\kappa[1+C(\omega)]-2i\omega} \quad (\text{S15})$$

and by the input-output relation Eq. S9 we obtain,

$$\tilde{b}_{\text{out}}(\omega) = \frac{-2ign\sqrt{\kappa}\alpha\Gamma e^{-\gamma\tau+i\omega\tau}}{\sqrt{2\pi}\{(i\gamma+\omega)^2+\Gamma^2/4\}\{\kappa[1+C(\omega)]-2i\omega\}} + t(\omega)\tilde{f}_{\text{spin}}(\omega) + r(\omega)\tilde{b}_{\text{in}}(\omega), \quad (\text{S16})$$

where

$$r(\omega) = \frac{\kappa[1-C(\omega)]+2i\omega}{\kappa[1+C(\omega)]-2i\omega}, \quad (\text{S17})$$

and

$$t(\omega) = \frac{2\kappa\sqrt{\text{Re}[C(\omega)]}}{\kappa[1+C(\omega)]-2i\omega} \quad (\text{S18})$$

are frequency dependent coefficients describing, respectively, the reflection on and transmission out of the cavity, and where we introduced the renormalized spin noise $\tilde{f}_{\text{spin}}(\omega) = \sqrt{\kappa\text{Re}[C(\omega)]}\tilde{F}_{\text{spin}}(\omega)$ obeying $[\tilde{f}_{\text{spin}}(\omega), \tilde{f}_{\text{spin}}^\dagger(\omega')] = \delta(\omega - \omega')$. We note that since $|t(\omega)|^2 = 1 - |r(\omega)|^2$ the spin noise term, $\tilde{f}_{\text{spin}}(\omega)$ ensures the correct commutator relations of the output field operators $\tilde{b}_{\text{out}}(\omega)$.

Equation (S16) clearly displays the mean amplitude and the quantum fluctuations of the output field from the resonator. In the experiment, the signal is integrated over a $T = 200\mu\text{s}$ time window. Since $T > 1/\kappa, 1/\Delta_{sq}, 1/\Gamma$, the sampled frequency components are within the cavity and squeezing bandwidths and they include the entire echo. We introduce a dimensionless field amplitude $b_{\text{mode}} = (1/\sqrt{T}) \int_{\tau-T/2}^{\tau+T/2} b_{\text{out}}(t) dt$, obeying oscillator commutator relations and being normalized such that $b_{\text{mode}}^\dagger b_{\text{mode}}$ is the photon number (operator) in the mode, and, e.g., the vacuum uncertainty on the associated amplitude quadratures is $1/2$. We introduce similarly the input $b_{\text{in}} = (1/\sqrt{T}) \int_{\tau-T/2}^{\tau+T/2} b_{\text{in}}(t) dt$ mode and $f_{\text{spin}} = (1/\sqrt{T}) \int_{\tau-T/2}^{\tau+T/2} f_{\text{spin}}(t) dt$, the transmitted spin noise in the temporal detection mode with $[f_{\text{spin}}, f_{\text{spin}}^\dagger] = 1$.

If the echo is fully contained within the square mode function, the corresponding amplitude b_{mode} is merely given by $\sqrt{2\pi/T}$ times $\tilde{b}_{\text{out}}(\omega = 0)$, i.e. the mean amplitude is

$$\beta_{\text{mode}} = \frac{-2ign\alpha e^{-\gamma\tau}}{\sqrt{\kappa T}[\Gamma^2/4 - \gamma^2][1 + C_n(0)]}. \quad (\text{S19})$$

This is purely imaginary, implying that the echo is fully contained in the mode quadrature $X_{\text{mode}} = \frac{1}{2i}(b_{\text{mode}} - b_{\text{mode}}^\dagger)$. From Eq. S16 one can show that the fluctuations in this quadrature are given by

$$\delta X_{\text{mode}}^2 = |r(0)|^2 \delta X_{\text{in}}^2 + \frac{(1 - |r(0)|^2)}{4} \left[\langle [f_{\text{spin}}, f_{\text{spin}}^\dagger] \rangle + 2 \langle f_{\text{spin}} f_{\text{spin}}^\dagger \rangle \right], \quad (\text{S20})$$

the sum of the fluctuations of the corresponding input mode quadrature $X_{\text{in}} = \frac{1}{2i}(b_{\text{in}} - b_{\text{in}}^\dagger)$ and of a contribution from the spin noise.

In a model where the spins are described as harmonic oscillators coupled via the F_j to an effective zero temperature bath, $[\langle [f_{\text{spin}}, f_{\text{spin}}^\dagger] \rangle + 2 \langle f_{\text{spin}} f_{\text{spin}}^\dagger \rangle]$ is equal to unity, while a more realistic description of the spins, taking into account the spin non-linearity as well as non-zero effective temperature, would yield a larger value but still of order unity. We thus conclude that the spin noise contribution is of order $(1 - |r(0)|^2)/4$.

In the limit of low cooperativity $C(0) \ll 1$, we find that $1 - |r(0)|^2 \simeq 4C(0)$, showing that the magnitude of fluctuations originating from the spins is given by the collective cooperativity which, in turn, is small ($C(0) \ll 1$) in our experiment. We will therefore neglect the spin contribution to the noise in the following paragraph, and come back to this term in Section IV of this Supplementary Material where we discuss the limitations of our scheme.

If the input field is squeezed, the quadrature measurements will have a variance given Eq. S6, and if the squeezing ellipse is properly aligned with the mean amplitude, this yields $\delta X_{\text{mode}}^2 = 1/(4G^2)$ so that the SNR is improved by the squeezing factor $\eta_S = G^2$ due to the squeezing. The finite bandwidth of the squeezing and of the resonator should, however, be taken into account in a more general calculation of the amplitude noise in the measurement. Note that even in the case of low collective cooperativity, the phase factor $(\kappa + 2i\omega)/(\kappa - 2i\omega)$ in Eq. S17 causes a relative rotation of the squeezing ellipse for different frequency components and hence a reduction of the effective squeezing of the field mode containing the echo signal.

Revisiting Eq. S16, we can determine the measured amplitude and noise for any arbitrary mode function. Note that these values are obtained in the post processing of the experimental data as an appropriate weighted average of the time dependent measured signal. Choosing a weighted mode function that matches the time dependent mean signal amplitude will thus yield a higher value of the weighted signal, while the noise may still be squeezed according

to Eq. S6.

III. EXPERIMENTAL DETAILS

A. Measurement setup

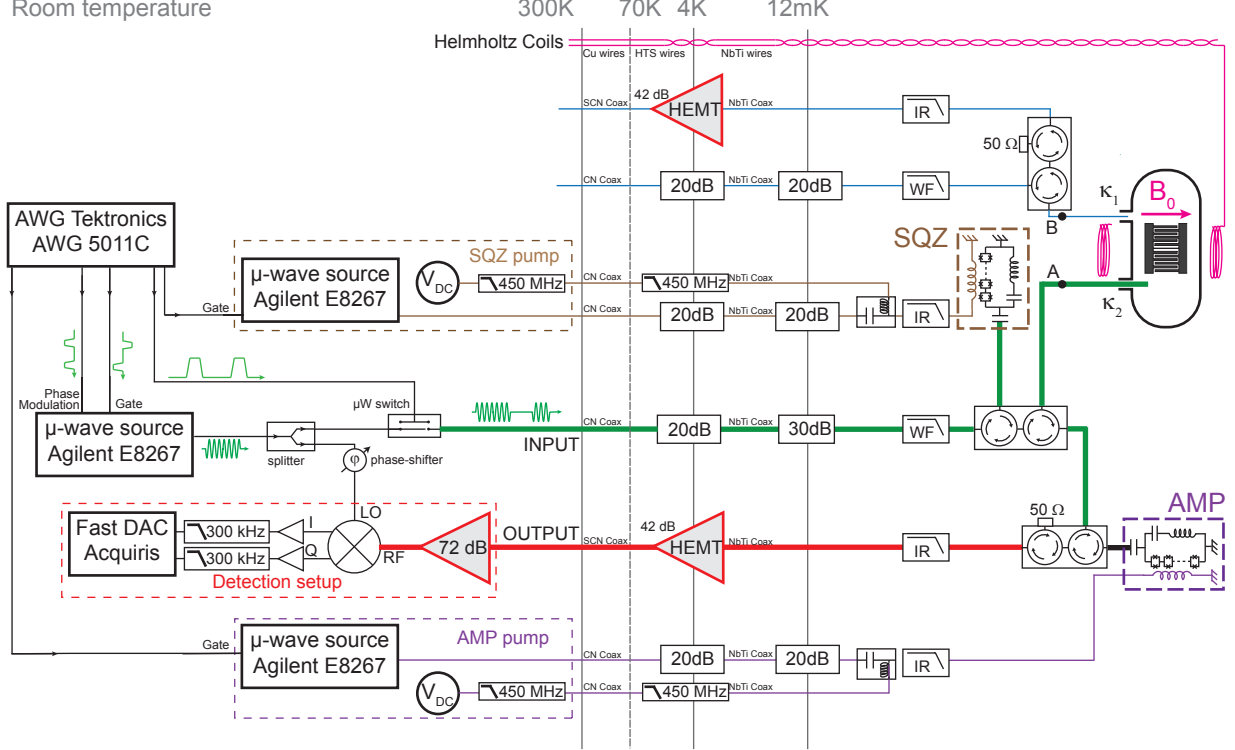


FIG. S1. Measurement setup

The detailed microwave setup is shown in Fig. S1. Although the resonator has two ports, it is largely overcoupled to port 2 since we designed $\kappa_2 \gg \kappa_1$ (see below). This port receives squeezed vacuum at its input generated by SQZ (green line in Fig. S1), and the field reflected on port 2 together with the spin-echo signal is routed to the amplifier (AMP) through the red line in Fig. S1, so that the green and red lines depict the setup schematized in Fig. 1b of the main text. The resonator design and fabrication details are given in [18]. The setup includes additional input-output lines to probe the LC resonator in reflexion on port 1 (blue lines), in transmission (blue-green lines), and in reflexion on port 2 (green-red lines). The coupling of the resonator to the measurement lines is done via the antennas inserted in the copper box, as shown in Fig. S2. Compared to ref. [18], antenna 2 was purposely made longer

in order to over-couple the resonator to port 2; conversely, to minimize coupling via port 1, antenna 1 was fully retracted (see Fig. S2), to achieve $\kappa_1 \ll \kappa_{int} \ll \kappa_2$. Measurement of the full resonator scattering matrix and a fit to the resonator input-output formulas [34] yields $\kappa_1 = 3 \cdot 10^3 \text{ s}^{-1}$, $\kappa_2 = 1.6 \cdot 10^6 \text{ s}^{-1}$ and $\kappa_{int} = 6 \cdot 10^4 \text{ s}^{-1}$ (see Fig. S2). Given that $\kappa_1 \ll \kappa_{int}$, we have not mentioned antenna 1 in the main text and used $\kappa_C = \kappa_2$ and $\kappa_L = \kappa_{int} + \kappa_1$.

Input lines are isolated from thermal photons by a minimum of 20 dB at 4 K and 20 dB at 20 mK, as well as commercial filters (Wavefade FLP0960). Output lines are protected from microwave noise by a minimum of two circulators and low-pass filters containing infra-red absorptive material. The ESR resonator and both JPAs are magnetically shielded, see [18] for details.

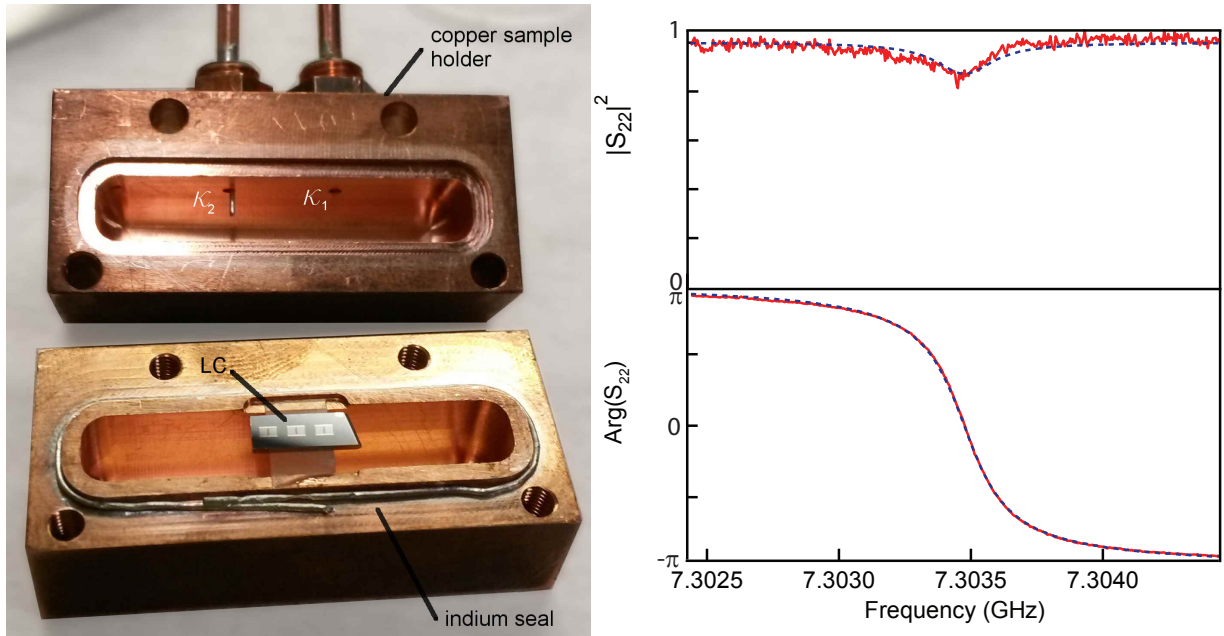


FIG. S2. **ESR resonator**(Left) Photograph of the copper sample holder showing the antenna asymmetry. The LC resonator is the aluminum circuit patterned on the silicon chip. The sample holder is made leak tight thanks to an indium seal, which ensures protection from stray infrared radiation that could increase resonator internal losses. (Right) Measured reflection coefficient S_{22} (red trace) and fit (dashed line), yielding the coupling rate κ_2 (corresponding to κ_C in the main text) as well as $\kappa_1 + \kappa_{int}$ (which we call κ_L in the main text)

The generation of the microwave pulses at the input and the detection setup are in every point similar to [18]. As explained in the main text, both AMP and SQZ have exactly the same design [20]. Both devices can be tuned to the desired operating frequency via a DC

bias of the flux threading their SQUID-array. The two microwave pump tones are generated by microwave sources locked with a 1 GHz synchronization loop to the microwave source providing the excitation pulses and the local-oscillator tone to ensure phase stability. The pump tones are in addition pulsed via the microwave source internal switches to generate gain only when needed.

B. Noise measurements and JPA limitations

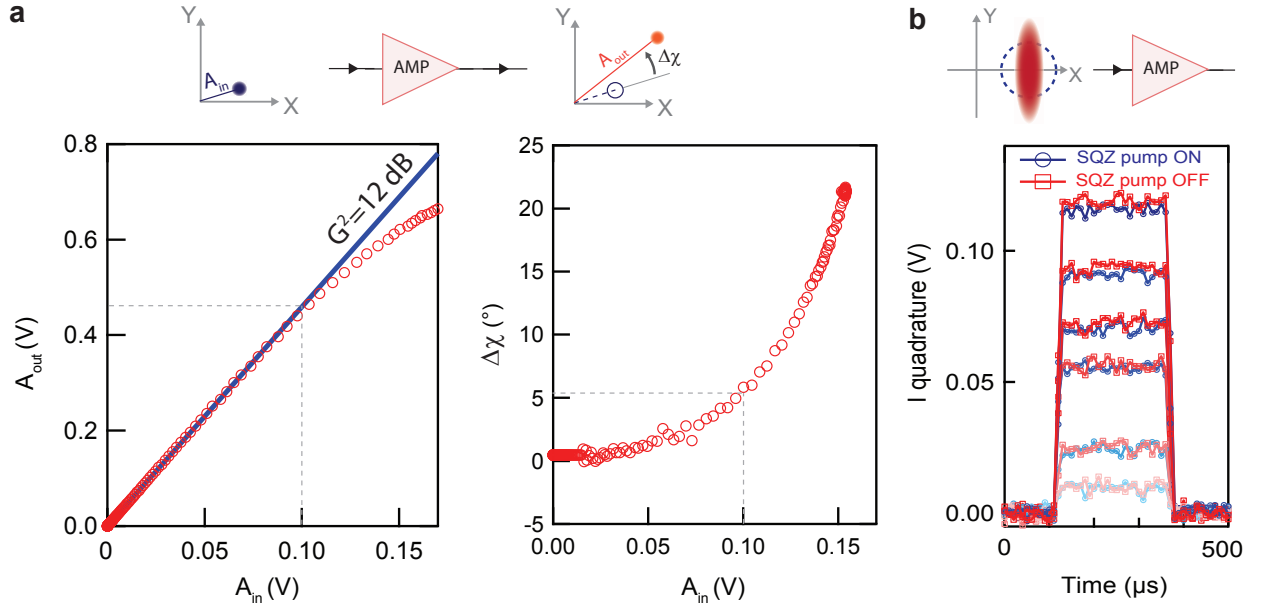


FIG. S3. **JPA non-linearity effects on amplification and squeezing.** (a) Measured amplitude and phase of a signal after amplification by the AMP device, in the same conditions as in the main text but operated in the non-degenerate mode, as a function of the input signal amplitude. A too strong input signal undergoes a phase shift due to the Josephson junctions non-linearity. This phase shift is already visible at approximately one third of the input amplitude at which the gain starts to saturate. (b) Comparison of averaged output signals obtained with SQZ off (red traces) and SQZ on (blue traces), for various input amplitudes of a weak microwave pulse sent via port 1. When the input amplitude reaches the level at which the phase shift evidenced in panel (a) is significant, the SQZ on and SQZ off average signals start differing from each other, whereas they are identical if the input amplitude stays below this value.

At the operation point chosen in the main text, in phase-preserving operation the AMP

has a bandwidth of 3 MHz and the SQZ a bandwidth of 4 MHz. These bandwidths are 10 times larger than the ESR resonator bandwidth κ and the detection bandwidth, chosen to be 300 kHz and set by the low-pass filters located in front of the acquisition card. As a consequence, we do not expect to see any effect of the limited bandwidth of the JPAs in our results. Characterization of the noise on one quadrature in the absence of a signal is achieved by acquiring a 500-ms-long time trace with a sampling rate of 100 kHz. The resulting 5×10^4 points are then used to generate a noise histogram, as shown for example in Fig. 2c of the main text, or estimate the variance of the signal, as shown in Fig. 2b of the main text. We have in addition checked that the noise distribution is well described by a Gaussian by verifying that all higher statistical moments are negligible.

As discussed in the main text, the saturation of the JPA devices represents an issue in several aspects of our experiment. When the current flowing through the Josephson junctions of the JPA's SQUID array approaches its critical value, the SQUID departs from the tunable inductor model with higher order terms appearing and inducing non-linearities in the device. At a given gain, the non-linearity limits the strength of the input signal that can be amplified. This effect can be observed by sending signals of increasing strength on the device. Fig. S3a shows results obtained for the AMP device operated in the same conditions as in the main text but in phase-preserving mode. On the left panel one can see that the output signal amplitude is limited to a threshold value (grey dashed line). More importantly for our experiment, the phase of the output signal is seen to deviate from the input signal at a threshold value three time less than the amplitude saturation.

This directly impacts the feasibility of the echo-detection scheme presented in the main text. As a squeezed coherent signal is a higher energy state than a non-squeezed coherent state of same amplitude, the squeezed state when amplified by the AMP has a larger phase deviation than the coherent state and thus the two states cannot be measured with the same quadrature choice and do not have the same measured amplitude. We observed this in our experiment by sending a small coherent pulse through port 1 of the ESR resonator, emulating the emission of an echo. Similarly to the main text, we can switch on and off the squeezing, generating squeezed and non-squeezed coherent states as depicted in Fig S3b. The phase of the detection is set to detect the non-squeezed state on the I quadrature. For large input signals, one can see that the SQZ on amplitude is a few percents lower than the SQZ off amplitude, because of the phase deviation discussed above. Such reduced mean

signal amplitude in presence of squeezing needs to be avoided; we thus intentionally choose to limit the amplitude of the emitted echo to avoid saturating the AMP. This is achieved by working on the tails of the spin distribution and having an excitation pulse of Rabi angle less than $\pi/2$ (we chose $\pi/3$ for the data shown in the main text).

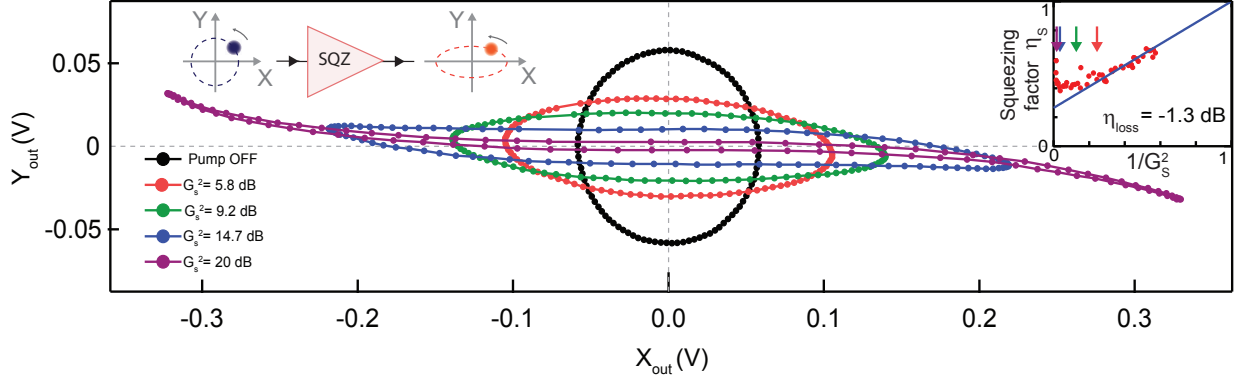


FIG. S4. **JPA non-linearity effects on squeezing.** Output quadratures X_{out} and Y_{out} of a small coherent signal sent to the SQZ measured for input phases ϕ_S spanning the whole interval between 0 and 2π , and corresponding measured squeezing factors η_S (inset), for various pump powers and hence gain G_S . At low pump power, the X_{out}, Y_{out} trajectory is well described by an ellipse, and η_S varies linearly with $1/G_S^2$. At a certain pump power, the ellipse becomes distorted and η_S stops decreasing with increasing gain G_S . For even higher gains, the trajectory becomes strongly distorted and η_S increases. Red, green, blue and purple arrows in the inset indicate the correspondence between the phase plane curves and the measured squeezing factors. Note that these data was taken in a simplified setup, where the ESR resonator and two circulators were removed compared to Fig. S1. A lower level of losses ($\eta_{loss} = -1.3$ dB) is thus extracted from the $\eta_S(G_S)$ fit, and a corresponding larger degree of squeezing is obtained $\eta_{s,min} = -3.8$ dB

The same phenomenon also limits the achievable degree of squeezing, as shown in Fig. S4. We measure the output quadratures X_{out} and Y_{out} of a weak input signal amplified by the SQZ in phase-sensitive mode as a function of its input phase. When the phase runs from 0 to 2π , plotting Y_{out} vs X_{out} emulates the shape of the produced squeezed vacuum. When the SQZ pump is off, a perfect circle is observed. At small or moderate gains (< 6 dB), the circle becomes an ellipse, with a small-axis projection which scales as G^{-2} (see red curve for instance). For larger gains however, the ellipse becomes strongly distorted inhibiting

further reduction of the "small-axis projection" (green and blue curves) and even causing it to increase (purple curve). We have thus chosen to use squeezing on the edge of the linear domain with $G_S^2 = 6$ dB (similar to the green curve) in the main text.

The data shown in Fig. S3 & S4 are obtained in a less complex setup where the ESR resonator and two circulators were removed. In this case, the losses are reduced to $\eta_{\text{loss}} = -1.3$ dB and a larger squeezing factor is obtained $\eta_S = -3.8$ dB. In the setup shown in Fig. S1, the losses arise from the 4 circulators (4×0.4 dB), the 2 m copper coaxial cables linking SQZ and AMP (0.5 dB) and the on-chips losses (LC 1 dB, SQZ and AMP 0.1 dB) and are compatible with the transmission factor $\eta_{\text{loss}} = -3.4$ dB measured in Fig. 2d of the main text.

C. ESR on Bismuth donors in Silicon

A neutral bismuth donor in silicon has spin properties arising from the coupling of the $\mathbf{S} = 1/2$ electronic spin to the ^{209}Bi $\mathbf{I} = 9/2$ nuclear spin. When placed in an external magnetic field \mathbf{B} , its twenty energy levels are described by the following spin Hamiltonian that includes a Zeeman effect for electronic and nuclear spin and an isotropic hyperfine coupling [35]:

$$H/\hbar = \mathbf{B} (\gamma_e \mathbf{S} \otimes \mathbb{1} - \gamma_n \mathbb{1} \otimes \mathbf{I}) + A \mathbf{S} \mathbf{I} \quad (\text{S21})$$

where $\gamma_e/2\pi = 27.997$ GHz/T and $\gamma_n/2\pi = 6.962$ MHz/T are the electronic and nuclear gyromagnetic ratios and $A/2\pi = 1.4754$ GHz is the hyperfine coupling constant[36]. The diagonalisation of the Hamiltonian as a function of \mathbf{B} yields the 20 energy levels shown in Fig. 1f of the main text. Labelling the energy levels by order of increasing energy $|i\rangle$, the transition probed in the main text is $|9\rangle \leftrightarrow |10\rangle$, as indicated by the blue arrow.

The sample is identical to the one presented in [22]. The bismuth atoms are implanted at 100-nm depth with a peak concentration of $[\text{Bi}] = 8.5 \times 10^{16} \text{cm}^{-3}$ and an activation yield of 60%.

D. Squeezing-enhanced echo: data acquisition and processing

We describe in the following the acquisition and post-processing of the echo data shown in Fig. 3(b and c) of the main text. To minimize setup drifts, we alternate echos acquired

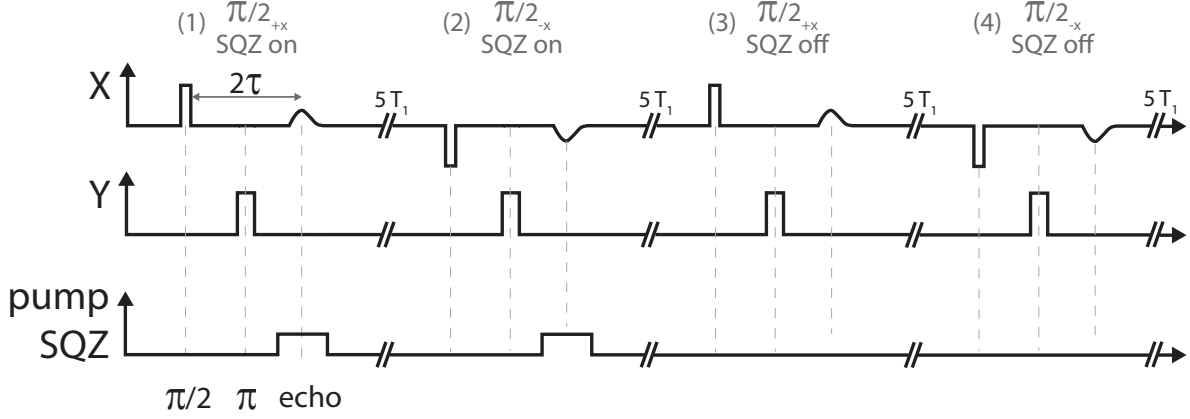


FIG. S5. **Experimental acquisition sequence** taken with $\tau = 200 \mu\text{s}$. Phase cycling as well as alternate SQZ switching are used to compensate setup drifts during the 6 h long acquisition.

with SQZ on and SQZ off as well as use phase-cycling, as shown in Fig. S5. We acquire $N_{avg} = 2500$ echos with SQZ on and 2500 SQZ off. The quadrature voltage $I(t)$ is digitalized at a sampling rate of $1\text{pt}/\mu\text{s}$ with an acquisition bandwidth of 300 kHz. The data is recorded on a time window $T = 200 \mu\text{s}$ centered on the echo. The waiting time between each echo sequence is taken to be $T_{rep} \approx 5T_1 = 5 \text{ s}$.

We compute the averaged signals shown in Fig. 3b of the main text as:

$$\bar{I}_{ON}(t) = \sum_{i=1}^{N_{avg}} \frac{I_{(1),i}(t) - I_{(2),i}(t)}{2} \text{ and } \bar{I}_{OFF}(t) = \sum_{i=1}^{N_{avg}} \frac{I_{(3),i}(t) - I_{(4),i}(t)}{2} \quad (\text{S22})$$

where subscripts (i) are denoted in Fig. S5. The noise histograms in Fig. 3c are computed from the bins $\{I_{(1),i}(t) - \bar{I}_{ON}(t), \forall i, \forall t\} \cup \{I_{(2),i}(t) + \bar{I}_{ON}(t), \forall i, \forall t\}$ when the SQZ is on and $\{I_{(3),i}(t) - \bar{I}_{OFF}(t), \forall i, \forall t\} \cup \{I_{(4),i}(t) + \bar{I}_{OFF}(t), \forall i, \forall t\}$. To ensure the echo emission is not affecting the noise properties, we have also computed the noise histograms and variances keeping only identical stamping times t and found no variations.

To compute the SNR for both echos, we define modes of the propagating field as $\langle O \rangle = \frac{1}{T} \langle O(t) \rangle u(t) dt$ with $u(t)$ a filter function normalized as $\frac{1}{T} \int [u(t)]^2 dt$ [18]. We pick as filter function the echo averaged signal $u(t) \propto [I_{ON}(t) + I_{OFF}(t)]/2$. For each echo $\{(n), i\}$, we can thus evaluate the signal and noise quantities as $\langle I_{(n),i} \rangle$ and $\sqrt{\langle \Delta I_{(n),i}^2 \rangle}$. Averaging over all recorded echos yields the noise and echo signal shown in Table I, demonstrating a noise reduction by 11%. Repeating the same procedure for a tophat u function of width $20 \mu\text{s}$ centered on the echo yields similar results.

$u(t)$	Echo shape			Top Hat function		
SQZ	$\langle I \rangle$	$\sqrt{\langle \Delta I^2 \rangle}$	SNR	$\langle I \rangle$	$\sqrt{\langle \Delta I^2 \rangle}$	SNR
OFF	0.179	0.202	0.886	0.161	0.202	0.797
ON	0.177	0.181	0.973	0.160	0.181	0.884
ON/OFF ratio	0.988	0.897	1.10	0.992	0.894	1.11

TABLE I. **Experimental results.**

E. Sensitivity estimate and numerical model

To estimate the sensitivity of the experiment and its improvement when using squeezed vacuum, we shall determine the number of spins contributing to the echo signal shown in Fig. 3 of the main text. This number is defined as the number of spins excited by the first $\pi/2$ pulse of the Hahn echo sequence. Due to the broadening of the line thanks to induced strain, the resonator bandwidth is 20 times smaller than the spin linewidth and we thus need to resort to numerical simulations as in our previous work [18] to obtain an estimate. The spin ensemble is modelled as N spin-1/2 systems coupled to the resonator with a Jaynes-Cummings Hamiltonian $H = \hbar g(a^\dagger \sigma_- + a \sigma_+)$, g being the spin-resonator coupling constant. Evolution of the spins observables and the intra-resonator field mean-values is then given by integrating the equations of motion given by the master equation of the system with a Markov approximation to take into account the resonator leakage and the spin decoherence [37]. To take into account the inhomogeneity in spin frequency and coupling constant, the spin ensemble is divided in M sub-ensembles with coupling constant $g^{(m)}$ and detuning to the resonator frequency $\Delta^{(m)}$.

In our former work, using the same sample and a resonator of same geometry, additional measurements such as the absorption of a weak microwave pulse and Rabi oscillations allowed to determine the spin distribution at $B_0 = 2.8$ mT (peak of the line) to be ideally modelled with a gaussian distribution in g of central value $g_0/2\pi = 56$ Hz and FWHM $\Delta g = 1.5$ Hz and a square distribution for the spin detunings with a width far exceeding the resonator bandwidth. Both distributions were weighted with a total overall factor $N_D = 3.6 \times 10^5$. Compared to [18], the resonator presented in the main text has a 10 times lower quality factor, corresponding to a 10 times larger linewidth and damping rate. Repeating the numerical simulations of [18] taking into account these modifications, we characterize the

number of spins contributing to the signal at $B_0 = 2.8$ mT to be $N_{\text{spins}} = 1.2 \times 10^5$.

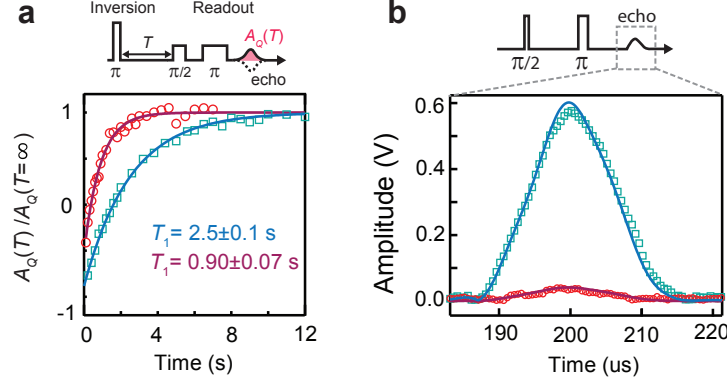


FIG. S6. **Calibration of number of excited spins.** In both panels, data acquired at $B_0 = 2.6$ mT ($B_0 = 2.8$ mT) are represented by red circles (blue squares) **a** Spin relaxation times measured using inversion recovery, well fit by exponential decays (solid lines). **b** Echo time traces reproduced via numerical simulations (solid lines).

The spin resonance frequency distribution is caused by strain applied by thermal contraction of the aluminium on the silicon substrate. As a result, the spin spectral and spatial distributions are linked [38]. Spins on the low-field side of the peak correspond to spins lying near the edge of the aluminium wire, whereas spins contributing to the $B_0 = 2.8$ mT peak correspond to spins located under the central part of the wire. Since the aluminium wire is superconducting, the current density is higher on the edge of the wire than in the central part, thus spins at $B_0 = 2.6$ mT are more strongly coupled to the resonator than spins at $B_0 = 2.8$ mT. To estimate the difference in g , we measure the spin relaxation time T_1 . As T_1 is radiatively limited by the Purcell effect in our experiment [25], we have $T_1^{-1} = 4g^2/\kappa$. Measuring T_1 at $B_0 = 2.6$ mT and $B_0 = 2.8$ mT (see Fig. S6a) and assuming that only the central value g_0 of the spin distribution should be adjusted, we find $g_0^{(\text{side})}/2\pi = 93$ Hz. The scaling of the overall weighting factor N_D is achieved by comparing the experimental echo amplitude at $B_0 = 2.6$ mT and $B_0 = 2.8$ mT (see Fig. S6b). Experimentally, we find a ratio $\alpha \approx \times 25$ and we adjust N_D until the simulated echo for $B_0 = 2.6$ mT is α times smaller than the echo simulated at $B_0 = 2.8$ mT. We find $N_D = 1.4 \times 10^4$ and thus the number of excited spins is $N_{\text{spins}} = 4.7 \times 10^3$.

Finally, we determine the sensitivity N_{min} defined in the main text as the minimum number of spins detected per echo with a SNR of 1. In the data shown in Fig. 3c of the

main text, the single-shot SNR is 0.37 in the absence of squeezing (see [18] and below for details on SNR evaluation) and we hence have $N_{\min} = N_{\text{spins}}/SNR = 1.3 \times 10^4$. This larger value compared to [18] is due to the lower quality factor of the resonator, as explained in Sec. IIIA of this Supplementary Material.

Thanks to these numerical simulations, we can also check the assumptions of low cooperativity made in Sec. II. Using the model corresponding to $B_0 = 2.6$ mT, we find $C = 0.002$, verifying $C \ll 1$ and thus confirming that the spin-noise contribution can be neglected at low squeezing.

IV. LIMITATIONS TO SQUEEZING-ENHANCED SENSITIVITY

We now wish to discuss theoretical limitations to squeezing-enhanced sensitivity. Indeed, should the technical issues described in Sec. IIIB be solved, arbitrary degrees of squeezing could be achieved. As we will see below, phenomena related to the presence of spins in the cavity and neglected so far would ultimately prevent the measurement sensitivity to increase without limit.

A first limitation is apparent in Eqs. S16 and S20. The output field variance is the sum of the input field variance reflected on the cavity and of the variance associated with the relaxation of the spins inside the cavity. At low squeezing, the first contribution is indeed reduced by squeezing the input field, but when the squeezed input noise contribution becomes of the same magnitude as the spin-noise contribution, no further increase in sensitivity will be obtained by squeezing the input field. Describing the spins as an ensemble of harmonic oscillators in coherent states relaxing via a zero-temperature bath as in the model presented in Section II, this limit is reached whenever $\eta_S = 1 - |r(0)|^2 \underset{C(0) \ll 1}{\simeq} 4C_n(0)$. In our experiment, the sensitivity would therefore no longer increase for a degree of input squeezing larger than 21 dB, corresponding to a maximum gain in sensitivity by a factor $\simeq 10$.

Besides modifying the output noise, squeezing may also affect the mean signal emitted by the spins, which constitutes yet another limitation to squeezing increased measurement sensitivity. Indeed, the mean components of a spin relax with rates that depend on the squeezed or thermal state of the radiation reservoir [11], while, for an oscillator, the reservoir state affects the Langevin noise terms rather than the relaxation rate, see, for example Eq. S10. We therefore have to abandon the oscillator description of the spins to estimate

their relaxation dynamics in the case of strong squeezing.

As suggested by Eq. S10, the cavity field quickly equilibrates to a squeezed state, and the spins hence experience an effective squeezed bath with the resonator bandwidth, which we assume smaller than bandwidth of the squeezed state from the JPA, $\kappa \leq \Delta_{sq}$. We approximate the effect of this bath on the individual mean spin components by the damping equations [11],

$$\begin{aligned}\langle \dot{\sigma}_x \rangle &= -\gamma_P(N + |M| + \frac{1}{2})\langle \sigma_x \rangle \\ \langle \dot{\sigma}_y \rangle &= -\gamma_P(N - |M| + \frac{1}{2})\langle \sigma_y \rangle \\ \langle \dot{\sigma}_z \rangle &= -2\gamma_P(N + \frac{1}{2})\langle \sigma_z \rangle - \gamma_P\end{aligned}\tag{S23}$$

where $\gamma_P = 4g^2/\kappa$ is the Purcell enhanced decay rate of the spin and where we assume x and y spin orientations for which the relevant squeezing parameters are N and $|M|$.

This treatment of the radiative damping of the mean spin components is not directly compatible with the Heisenberg operator equations of motion, but it shows that the mean spin components and in particular $\langle \sigma_z \rangle$ decays faster in the presence of squeezing, and that its steady-state value is reduced by a factor $1/(1 + 2N)$, which will directly impact the spin-echo signal amplitude as verified in Fig. 4 of the main text. As demonstrated in the main text, we may apply the squeezed radiation only in a time window of a few $1/\Gamma$ around the echo pulse, and hence benefit from the squeezing as long as $2\gamma_P(N + 1/2) \ll T_E^{-1}$, i.e. $N \ll T_1/(2T_E)$. This simple criterion shows that for our spin and cavity parameters, two orders of magnitude improvement of the SNR may be achieved if we can prepare the correspondingly squeezed input field.

Overall, and for our experimental parameters, the most stringent limitation to squeezing enhanced sensitivity seems to be the spin-noise contribution. This can be traced to the fact that this limitation becomes relevant when η_S reaches the collective cooperativity level (squeezing is efficient in reducing the output noise as long as $\eta_S > 4C(0)$), whereas the second criterion $\eta_S > C_1/2$, concerning the reduced mean signal in the presence of squeezing, involves only the much smaller single-spin cooperativity $C_1 = 4g^2/(\kappa\Gamma)$.

A more complete analysis, relying on the numerical method applied in [39], will be needed to find the exact theoretical limitation if arbitrary squeezing can be achieved.

V. CHARACTERIZATION OF THE MEAN NUMBER OF THERMAL PHOTONS

In order to produce a squeezed vacuum state of the field b_{in} that serves as input to the ESR resonator, the squeezer "SQZ" is pumped while its input is in the vacuum state (see Fig. S1). However, due to imperfect filtering of the microwave probe lines and to the refrigerator finite base temperature, one can never reach perfect electromagnetic vacuum. In this section, we describe the calibration procedure used to place an upper bound on the average excitation number of the input modes $b_{\text{in}}[\omega]$ around the ESR resonator resonance frequency (typically $|\omega - \omega_0| \leq \kappa_c$) when the squeezer is off. Note that this average excitation number is in fact characterized at a slightly different frequency $\omega_1/2\pi = 7.62$ GHz, but we assume that the thermal equilibrium is similar so that $\langle b_{\text{in}}^\dagger[\omega]b_{\text{in}}[\omega] \rangle = \langle b_{\text{in}}^\dagger[\omega_1]b_{\text{in}}[\omega_1] \rangle$ for all relevant values of ω . This assumption is reasonable given that $|\omega - \omega_1| \ll k_B T$ (either T being the refrigerator base temperature, or the effective temperature of the modes given at the end of this section), and the transmission of the microwave input lines is flat (± 0.5 dB) variation) on this frequency range.

The method consists in replacing, in a subsequent cool-down of the refrigerator, the ESR resonator with a transmon superconducting qubit [40] coupled to a microwave readout resonator with resonance frequency ω_1 . The resonator-qubit system is in the so-called *strong dispersive regime* of circuit QED in which photons in the resonator mode lead to dephasing of the qubit [41, 42]. Thus, by measuring the dephasing rate of the qubit beyond the effect of population relaxation $\gamma_\phi = \gamma_2 - \gamma_1/2$, one can place an upper bound on the thermal photon number in the readout resonator, and then on the occupation of the traveling modes b_{in} .

The device that we use was not designed specifically for the experiment, but was studied in Ref. [43]. On a sapphire chip, 4 lumped element microwave readout resonators, each one capacitively coupled to a transmon qubit (see Fig. S7), are coupled to a single transmission feedline. In the following, we consider only the qubit-resonator system labeled *cell 2* (the other ones are well out of resonance). The feedline is connected to the setup depicted on Fig. S1 at points A and B. Note that in this geometry, the readout resonator thermal occu-

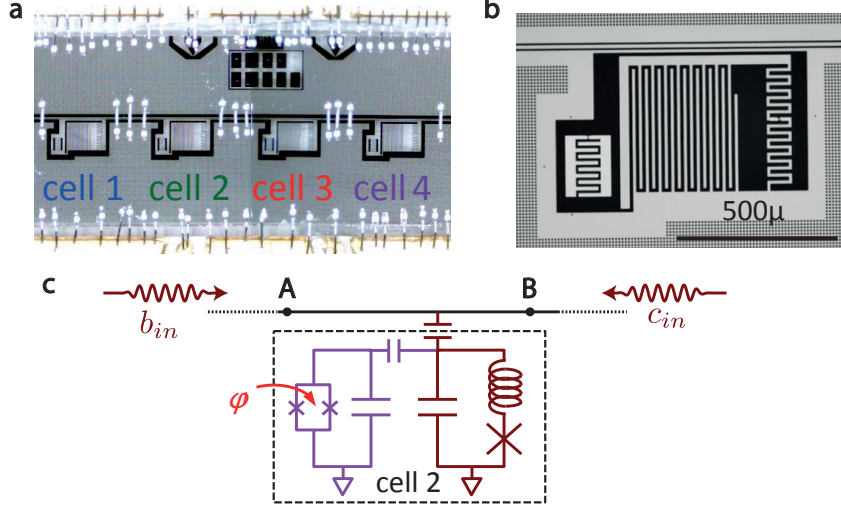


FIG. S7. **a)** Optical micrograph of the device used for estimating the number of thermally excited photons in b_{in} . Four cells, each one composed of a transmon qubit with an attached readout resonator are probed with a single microwave feedline. **b)** Zoom on one of the cells, showing the tunable transmon qubit (to the left) capacitively coupled to the readout resonator (to the right), itself capacitively coupled to the feedline (to the top). **c)** Simplified electric circuit of the cell used for the calibration. The qubit contains a split Josephson junction and its resonance frequency can be tuned by threading the loop with a magnetic flux φ . The resonator, which contains an array of junctions, is slightly non linear. Thermal excitations in the resonator are due to both right and left traveling modes b_{in} and c_{in} in the feedline.

pation is set by the average occupation of right propagating modes b_{in} through A and left propagating modes c_{in} through B (see Fig. S7 a). Internal losses of the readout resonator, that could act as a coupling to a fictitious cold reservoir, are shown to be negligible on Fig. S9 d. The blue input line connected at B on Fig. S1, which was originally designed to probe the ESR resonator in reflection on port 1, is less attenuated by 10 dB than the green line connected to A so that left propagating modes tend to increase the thermal occupation of the readout resonator. This issue does not arise with the ESR resonator since the coupling rate through port 1 is negligible ($\kappa_1 \ll \kappa_2$). Thus, the calibration made here is conservative and the estimation of the thermal occupation of b_{in} is considered as an upper bound of the actual value in the experiment.

The readout resonator consists in an interdigitated capacitor made out of superconducting aluminum in parallel of an array of Josephson junctions (Fig. S7). This array behaves as a non-linear inductor and was originally designed to allow for a single-shot readout of the attached qubit. This non-linearity is not relevant here and can anyway be neglected as the average photon number in the resonator is well below one. The transmon qubit is made out of a smaller interdigitated capacitor in parallel with a split Josephson junction that allows to tune its resonance frequency. A DC magnetic field is then applied using a superconducting coil in order to operate the device at its *sweet spot*, where its frequency $\omega_q/2\pi = 6.23$ GHz does not depend on the magnetic field fluctuations at first order (see Fig. S8).

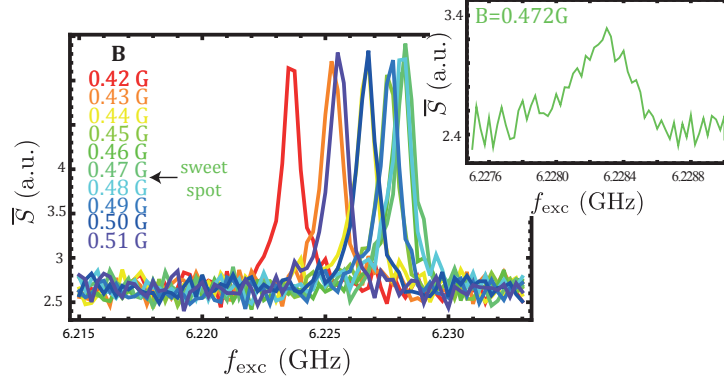


FIG. S8. **Two-tone spectroscopy** of the qubit. Starting from thermal equilibrium, the qubit is shined with a $5 \mu\text{s}$ -long saturating pulse (power -20 dBm referenced at refrigerator input) of frequency f_{exc} and then readout with an optimized pulse around $\omega_1/2\pi$ (see text and Fig. S9). The integrated signal \bar{S} reveals the qubit excited state occupation. One can vary the qubit resonance frequency by varying the amplitude of the applied B-field (encoded in color). **Inset:** desaturated qubit resonance (power -30 dBm at fridge input) at the sweet spot, showing that $\omega_q/2\pi = 6.228$ GHz.

The coupling rate of the qubit and readout resonator is much smaller than the detuning $\omega_1 - \omega_q$ so that the system is described by the dispersive hamiltonian [42]

$$H = \hbar\omega_1(a^\dagger a + \frac{1}{2}) + \hbar\omega_q \frac{\sigma_z}{2} + \hbar\chi a^\dagger a \sigma_z. \quad (\text{S24})$$

Here, σ_z is the Pauli operator of the qubit and χ is the qubit state dependent shift of

the readout resonator frequency, which provides us with a robust readout method of the transmon[44, 45]. Indeed, by probing the resonator with a near resonant microwave and integrating a quadrature of the transmitted field, one gets a signal \bar{S} depending linearly on $\langle\sigma_z\rangle$. In practice, the power, duration and frequency of the readout pulse was empirically adjusted to optimize signal-to-noise ratio. It corresponds to few photons in the resonator (power 10 dB larger than for 1 photon characterization of the resonator on Fig S9 d). Note that the amplifier JPA was turned off during all measurements.

In Ref. [46], Rigetti *et al.* computed the dephasing rate of a qubit induced by thermally excited photons in the readout resonator mode. It reads

$$\gamma_{\text{phot}} = \frac{\kappa}{2} \text{Re}\left\{\left((1 + 2i\frac{\chi}{\kappa})^2 + 8i\bar{n}\frac{\chi}{\kappa}\right)^{1/2} - 1\right\}, \quad (\text{S25})$$

where κ is the photon exit rate from the readout resonator, and $\bar{n} = \langle a^\dagger a \rangle$ is the mean number of photons hosted by the resonator. Considering that $\gamma_{\text{phot}} \leq \gamma_\phi = \gamma_2 - \gamma_1/2$, we now measure the qubit population and coherence relaxation rates γ_1 and γ_2 as well as all parameters entering the expression S25 in order to place an upper bound on \bar{n} .

By applying π and $\pi/2$ excitation pulses (calibrated by recording Rabi oscillations of the qubit), we first measure the qubit population relaxation rate $\gamma_1 = 0.41 \mu\text{s}^{-1}$ (see Fig. S9 a) and coherence relaxation rate $\gamma_2^* = 1.1 \mu\text{s}^{-1}$ (see Fig. S9 b). This last rate corresponds to a free-induction decay measurement, and includes the effect of low-frequency noise, such as second order effects of the fluctuations in the flux threading the qubit loop, along with high-frequency noise induced by thermal photons in the readout resonator. A Hahn-echo measurement, yielding a decay rate $\gamma_{2,\text{echo}} \simeq \gamma_2^*$ shows that the former is negligible compared to the latter (see Fig. S9 c). We can then extract the qubit pure dephasing rate $\gamma_\phi = \gamma_2 - \gamma_1/2 = 0.9 \mu\text{s}^{-1}$.

In order to measure precisely χ , we then detect the transmitted signal through the feedline for a probe pulse of low amplitude (linear regime of the readout resonator) and integrate the signal over $0.2 \mu\text{s} \ll T_1$ in the stationary regime of the resonator (signal during ring-up is discarded in order to avoid distortion of the signal). The transmission coefficient from A

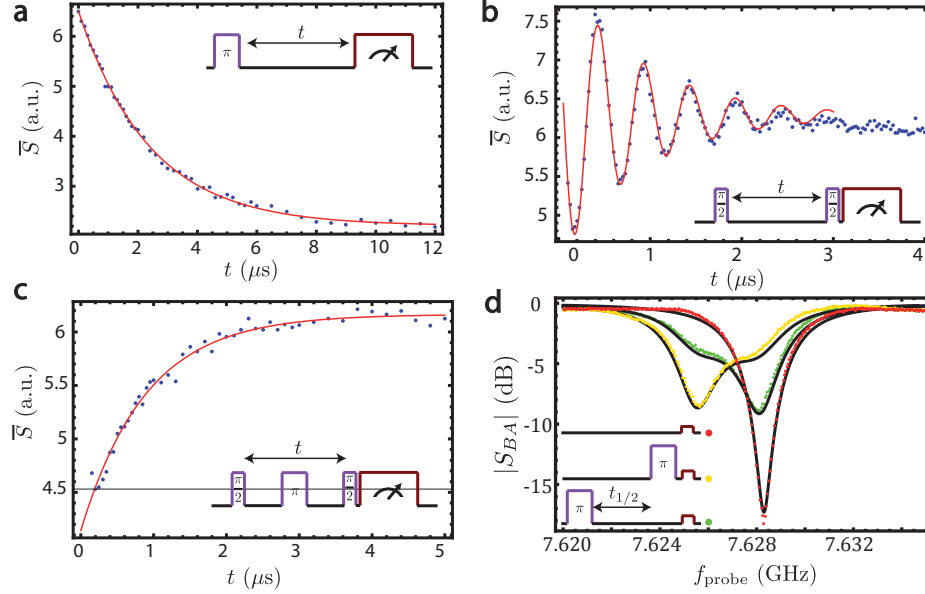


FIG. S9. **Qubit-resonator parameters characterization.** For each measurement, the pulse sequence is schematically represented at ω_q (in purple, all rotations around σ_y of the qubit) and at $\omega_{\text{readout}} \simeq \omega_1$ (in brown). **a)** Population relaxation measurement yielding $T_1 = 2.4 \mu\text{s}$, **b)** Free induction decay measurement yielding $T_2^* = 0.9 \mu\text{s}$ (excitation pulses at $\omega_q/2\pi + 2 \text{ MHz}$). **c)** Hahn-echo measurement yielding $T_{2,\text{echo}} = 0.9 \mu\text{s}$. **d)** Measured transmission coefficient S_{AB} when the qubit is at thermal equilibrium (red dots), right after an inverting π -pulse (yellow dots) and a qubit half-life later (green dots). Black lines: global fit with parameters $p_\pi = 0.66$, $\chi/2\pi = 1.48 \text{ MHz}$ and $\kappa_{\text{int}}/\kappa_{\text{ext}} = 0.14$. For **a**, **b** and **c** the readout pulse power is empirically adjusted to optimize signal to noise ratio and the transmitted field is integrated over $5 \mu\text{s}$. Only the quadrature \bar{S} containing information on the qubit state is plotted. For **d** the readout pulse power is low enough that readout resonator non-linearity is neglected and the transmitted field is integrated over $0.2 \mu\text{s}$ in the stationary regime.

to B then reads[47]

$$S_{BA}(\omega) = p \frac{\kappa_{\text{int}} + 2i(\omega - \omega_{\text{res}} - \chi)}{\kappa_{\text{int}} + \kappa_{\text{ext}} + 2i(\omega - \omega_{\text{res}} - \chi)} + (1-p) \frac{\kappa_{\text{int}} + 2i(\omega - \omega_{\text{res}} + \chi)}{\kappa_{\text{int}} + \kappa_{\text{ext}} + 2i(\omega - \omega_{\text{res}} + \chi)}, \quad (\text{S26})$$

where κ_{ext} (resp. κ_{int}) is the resonator photon exit rate into the feedline (resp. due to internal losses) and $p = \langle 1 - \sigma_z \rangle / 2$ is the occupation of the ground state of the qubit. Note that the total photon exit rate from the resonator $\kappa = \kappa_{\text{int}} + \kappa_{\text{ext}} = 2.04 \times 10^7 \text{ s}^{-1}$ is determined independently by measuring the ringdown time of the resonator.

We record this transmission coefficient at thermal equilibrium ($p \simeq 1$, red dots on Fig. S9 d),

after applying a π -pulse ($p = p_\pi$, yellow dots) and, for better precision, a duration $t_{1/2} = \ln 2 T_1$ after the same pulse ($p = p_\pi/2$, green dots). If p_π can be roughly estimated given the drive pulse duration and delay before signal integration, it is difficult to predict accurately its value due to the reduction of T_1 in presence of a field in the readout resonator[48]. We rather estimate it along with the other parameters entering Eq. S26 by fitting these three curves altogether (black curves), which yields $p_\pi = 0.66$, $\chi/2\pi = 1.48$ MHz and $\kappa_{\text{int}}/\kappa_{\text{ext}} = 0.14$. In this fit, we allow for a global scaling factor accounting for the attenuation in the lines, and a small offset in the transmitted field complex amplitude, attributed to impedance mismatch.

From this calibration and using Eq. S25, we find for the readout resonator $\bar{n}_{\text{res}} \leq 0.1$. As mentioned in the beginning of this section, it is a conservative estimate of the average thermal photon number in the ESR resonator mode when the squeezer is off.

For a thermal state of an harmonic oscillator, the fluctuations on one quadrature read

$$\begin{aligned} \langle \delta X^2 \rangle &= \text{Tr}[\rho_{th}(\frac{a+a^\dagger}{2})^2] \\ &= (1 + 2\text{Tr}[\rho_{th}a^\dagger a])/4 \\ &= (1 + 2\bar{n})/4. \end{aligned} \tag{S27}$$

In the experiment, following Fig. 2d of the main text, the detected output noise is reduced when the squeezer is on as $\langle \delta I^2 \rangle_{\text{on}} / \langle \delta I^2 \rangle_{\text{off}} = 0.75$. Then, the fluctuations of the squeezed quadrature verify $\langle \delta X^2 \rangle_{\text{on}} / \langle \delta X^2 \rangle_{\text{off}} < 0.75$, so that $\langle \delta X^2 \rangle_{\text{on}} < 0.75(1 + 2\bar{n}_{\text{ESR}})/4 < 0.225$, which is below the vacuum fluctuations level $\langle \delta I^2 \rangle_{\text{vac}} = 1/4$.

When subtracting the background noise $\langle \delta I^2 \rangle_{bg}$ obtained when both SQZ and AMP are switched off, one gets a more stringent condition $\langle \delta X^2 \rangle_{\text{on}} / \langle \delta X^2 \rangle_{\text{off}} < \frac{\langle \delta I^2 \rangle_{\text{on}} - \langle \delta I^2 \rangle_{bg}}{\langle \delta I^2 \rangle_{\text{off}} - \langle \delta I^2 \rangle_{bg}} = 0.66$, (see Fig. 2 d), which corresponds to a reduction of -1 dB below the vacuum fluctuations for the squeezed quadrature.

-
- [1] Carlton M. Caves, “Quantum-mechanical noise in an interferometer,” *Phys. Rev. D* **23**, 1693–1708 (1981).
- [2] P. Grangier, R. E. Slusher, B. Yurke, and A. LaPorta, “Squeezed-light enhanced polarization interferometer,” *Phys. Rev. Lett.* **59**, 2153–2156 (1987).
- [3] Min Xiao, Ling-An Wu, and H. J. Kimble, “Precision measurement beyond the shot-noise limit,” *Phys. Rev. Lett.* **59**, 278–281 (1987).
- [4] LIGO Scientific Collaboration, “A gravitational wave observatory operating beyond the quantum shot-noise limit,” *Nature Physics* **7**, 962–965 (2011).
- [5] Junaid Aasi, J Abadie, BP Abbott, Richard Abbott, TD Abbott, MR Abernathy, Carl Adams, Thomas Adams, Paolo Addesso, RX Adhikari, *et al.*, “Enhanced sensitivity of the ligo gravitational wave detector by using squeezed states of light,” *Nature Photonics* **7**, 613–619 (2013).
- [6] E. S. Polzik, J. Carri, and H. J. Kimble, “Spectroscopy with squeezed light,” *Phys. Rev. Lett.* **68**, 3020–3023 (1992).
- [7] Nicolas Treps, Nicolai Grosse, Warwick P Bowen, Claude Fabre, Hans-A Bachor, and Ping Koy Lam, “A quantum laser pointer,” *Science* **301**, 940–943 (2003).
- [8] Vito Giovanni Lucivero, Ricardo Jiménez-Martínez, Jia Kong, and Morgan W. Mitchell, “Squeezed-light spin noise spectroscopy,” *Phys. Rev. A* **93**, 053802 (2016).
- [9] Michael A Taylor, Jiri Janousek, Vincent Daria, Joachim Knittel, Boris Hage, Hans-A Bachor, and Warwick P Bowen, “Biological measurement beyond the quantum limit,” *Nature Photonics* **7**, 229–233 (2013).
- [10] R. Movshovich, B. Yurke, P. G. Kaminsky, A. D. Smith, A. H. Silver, R. W. Simon, and M. V. Schneider, “Observation of zero-point noise squeezing via a josephson-parametric amplifier,” *Physical Review Letters* **65**, 1419–1422 (1990).
- [11] C. W. Gardiner, “Inhibition of atomic phase decays by squeezed light: A direct effect of squeezing,” *Phys. Rev. Lett.* **56**, 1917–1920 (1986).
- [12] KW Murch, SJ Weber, KM Beck, Eran Ginossar, and I Siddiqi, “Reduction of the radiative decay of atomic coherence in squeezed vacuum,” *Nature* **499**, 62–65 (2013).
- [13] DM Toyli, AW Eddins, S Boutin, S Puri, D Hover, V Bolkhovsky, WD Oliver, A Blais, and I Siddiqi, “Resonance fluorescence from an artificial atom in squeezed vacuum,” arXiv preprint

- arXiv:1602.03240 (2016).
- [14] J.B. Clark, F. Lecoq, R.W. Simmonds, J. Aumentado, and J.D. Teufel, *Nature Phys.* (2016).
 - [15] Nicolas Didier, Archana Kamal, William D. Oliver, Alexandre Blais, and Aashish A. Clerk, “Heisenberg-limited qubit read-out with two-mode squeezed light,” *Phys. Rev. Lett.* **115**, 093604 (2015).
 - [16] Nicolas Didier, Jérôme Bourassa, and Alexandre Blais, “Fast quantum nondemolition readout by parametric modulation of longitudinal qubit-oscillator interaction,” *Phys. Rev. Lett.* **115**, 203601 (2015).
 - [17] Vittorio Giovannetti, Seth Lloyd, and Lorenzo Maccone, “Quantum-enhanced measurements: beating the standard quantum limit,” *Science* **306**, 1330–1336 (2004).
 - [18] A Bienfait, J.J. Pla, Y. Kubo, M. Stern, X. Zhou, C.-C. Lo, C.D. Weis, T. Schenkel, M.L.W. Thewalt, D. Vion, D. Esteve, B. Julsgaard, K. Moelmer, J.J.L. Morton, and P. Bertet, “Reaching the quantum limit of sensitivity in electron spin resonance,” *Nature Nanotechnology* **11**, 253 – 257 (2015).
 - [19] E.L. Hahn, “Spin echoes,” *Phys. Rev.* **80**, 580–594 (1950).
 - [20] X. Zhou, V. Schmitt, P. Bertet, D. Vion, W. Wustmann, V. Shumeiko, and D. Esteve, “High-gain weakly nonlinear flux-modulated josephson parametric amplifier using a squid array,” *Phys. Rev. B* **89**, 214517 (2014).
 - [21] Gary Wolfowicz, Alexei M Tyryshkin, Richard E George, Helge Riemann, Nikolai V Abrosimov, Peter Becker, Hans-Joachim Pohl, Mike LW Thewalt, Stephen A Lyon, and John JL Morton, “Atomic clock transitions in silicon-based spin qubits,” *Nature nanotechnology* **8**, 561–564 (2013).
 - [22] C. D. Weis, C. C. Lo, V. Lang, A. M. Tyryshkin, R. E. George, K. M. Yu, J. Bokor, S. A. Lyon, J. J. L. Morton, and T. Schenkel, “Electrical activation and electron spin resonance measurements of implanted bismuth in isotopically enriched silicon-28,” *Applied Physics Letters* **100**, 172104 (2012).
 - [23] F. Mallet, M. A. Castellanos-Beltran, H. S. Ku, S. Glancy, E. Knill, K. D. Irwin, G. C. Hilton, L. R. Vale, and K. W. Lehnert, “Quantum state tomography of an itinerant squeezed microwave field,” *Physical Review Letters* **106**, 220502 (2011).
 - [24] J.J. Pla, A. Bienfait, G. Pica, J. Mansir, F.A. Mohiyaddin, A. Morello, T. Schenkel, B.W. Lovett, J.J.L. Morton, and P. Bertet, arXiv:1608.07346 (2016).

- [25] A. Bienfait, J.J. Pla, Y. Kubo, X. Zhou, M. Stern, C.-C. Lo, C.D. Weis, T. Schenkel, D Vion, D. Esteve, J.J.L. Morton, and P. Bertet, “Controlling spin relaxation with a cavity,” *Nature* **531**, 74 – 77 (2016).
- [26] T. Sleator, E. L. Hahn, C. Hilbert, and J. Clarke, “Nuclear-spin noise,” *Phys. Rev. Lett.* **55**, 1742–1745 (1985).
- [27] K.W. Murch, S.J. Weber, C. Macklin, and I. Siddiqi, “Observing single quantum trajectories of a superconducting quantum bit,” *Nature* **502**, 211 (2013).
- [28] A.M. Tyryshkin, S. Tojo, J.L. Morton, H. Riemann, N.V. Abrosimov, P. Becker, H.-J. Pohl, T. Schenkel, M.L.W. Thewalt, K.M. Itoh, and S.A. Lyon, “Electron spin coherence exceeding seconds in high-purity silicon,” *Nature Materials* **11**, 143–147 (2012).
- [29] Joseph Kerckhoff, Kevin Lalumière, Benjamin J. Chapman, Alexandre Blais, and K. W. Lehnert, “On-chip superconducting microwave circulator from synthetic rotation,” *Phys. Rev. Applied* **4**, 034002 (2015).
- [30] Adrien Facon, Eva-Katharina Dietsche, Dorian Grosso, Serge Haroche, Jean-Michel Raimond, Michel Brune, and Sébastien Gleyzes, “A sensitive electrometer based on a rydberg atom in a schrödinger-cat state,” *Nature* **535**, 262–265 (2016).
- [31] C. W. Gardiner and P. Zoller, *Quantum Noise*, 2nd ed. (Springer, Berlin, 2000).
- [32] C. W. Gardiner and M. J. Collett, “Input and output in damped quantum systems: Quantum stochastic differential equations and the master equation,” *Phys. Rev. A* **31**, 3761 (1985).
- [33] T. Holstein and H. Primakoff, “Field dependence of the intrinsic domain magnetization of a ferromagnet,” *Phys. Rev.* **58**, 1098 (1940).
- [34] A. Palacios-Laloy, Superconducting qubit in a resonator : test of the Leggett-Garg inequality and single-shot readout (2010).
- [35] R. E. George, W. Witzel, H. Riemann, N. V. Abrosimov, N. Nötzel, M. L. W. Thewalt, and J. J. L. Morton, “Electron spin coherence and electron nuclear double resonance of bi donors in natural si,” *Phys. Rev. Lett.* **105**, 067601 (2010).
- [36] Gavin W Morley, Marc Warner, A Marshall Stoneham, P Thornton Greenland, Johan van Tol, Christopher WM Kay, and Gabriel Aeppli, “The initialization and manipulation of quantum information stored in silicon by bismuth dopants,” *Nature materials* **9**, 725–729 (2010).
- [37] C. Grezes, B. Julsgaard, Y. Kubo, M. Stern, T. Umeda, J. Isoya, H. Sumiya, S. Abe, S. Onoda, T. Ohshima, V. Jacques, J. Esteve, D. Vion, D. Esteve, K. Moelmer, and P. Bertet,

- “Multimode storage and retrieval of microwave fields in a spin ensemble,” *Phys. Rev. X* **4**, 021049 (2014).
- [38] J. J. Pla, A. Bienfait, G. Pica, J. Mansir, F. A. Mohiyaddin, A. Morello, T. Schenkel, B. W. Lovett, J. J. L. Morton, and P. Bertet, “Strain-induced nuclear quadrupole splittings in silicon devices,” .
- [39] Brian Julsgaard and Klaus Moelmer, “Dynamical evolution of an inverted spin ensemble in a cavity: Inhomogeneous broadening as a stabilizing mechanism,” **86**, 10.1103/Phys-RevA.86.063810.
- [40] Jens Koch, M Yu Terri, Jay Gambetta, Andrew A Houck, DI Schuster, J Majer, Alexandre Blais, Michel H Devoret, Steven M Girvin, and Robert J Schoelkopf, “Charge-insensitive qubit design derived from the cooper pair box,” *Physical Review A* **76**, 042319 (2007).
- [41] Jay Gambetta, Alexandre Blais, David I Schuster, Andreas Wallraff, L Frunzio, J Majer, Michel H Devoret, Steven M Girvin, and Robert J Schoelkopf, “Qubit-photon interactions in a cavity: Measurement-induced dephasing and number splitting,” *Physical Review A* **74**, 042318 (2006).
- [42] Alexandre Blais, Jay Gambetta, A Wallraff, DI Schuster, SM Girvin, MH Devoret, and RJ Schoelkopf, “Quantum-information processing with circuit quantum electrodynamics,” *Physical Review A* **75**, 032329 (2007).
- [43] Vivien Schmitt, X Zhou, K Juliusson, B Royer, Alexandre Blais, Patrice Bertet, Denis Vion, and D Esteve, “Multiplexed readout of transmon qubits with josephson bifurcation amplifiers,” *Physical Review A* **90**, 062333 (2014).
- [44] A Wallraff, DI Schuster, A Blais, L Frunzio, J Majer, MH Devoret, SM Girvin, and RJ Schoelkopf, “Approaching unit visibility for control of a superconducting qubit with dispersive readout,” *Physical review letters* **95**, 060501 (2005).
- [45] MD Reed, L DiCarlo, BR Johnson, L Sun, DI Schuster, L Frunzio, and RJ Schoelkopf, “High-fidelity readout in circuit quantum electrodynamics using the jaynes-cummings nonlinearity,” *Physical review letters* **105**, 173601 (2010).
- [46] Chad Rigetti, Jay M Gambetta, Stefano Poletto, BLT Plourde, Jerry M Chow, AD Córcoles, John A Smolin, Seth T Merkel, JR Rozen, George A Keefe, et al., “Superconducting qubit in a waveguide cavity with a coherence time approaching 0.1 ms,” *Physical Review B* **86**, 100506 (2012).

- [47] David M Pozar, Microwave engineering (John Wiley & Sons, 2009).
- [48] Maxime Boissonneault, Jay M Gambetta, and Alexandre Blais, “Dispersive regime of circuit qed: Photon-dependent qubit dephasing and relaxation rates,” *Physical Review A* **79**, 013819 (2009).